Ludwig-Maximilians-Universität München

Faculty of Physics

Max-Planck-Institute for Astrophysics

Master's Degree in Astrophysics

Master Thesis

Theoretical Predictions for the Surface Magnetic Fields of Binary-stripped Massive Stars

Advisors

Prof. Dr. Selma E. de Mink

Jing-Ze Ma

Collaborator

Prof. Dr. Ylva Götberg

Candidate

Giovanni Stimamiglio

Summer Semester 2025

Ludwig-Maximilians-Universität München

Fakultät für Physik

Max-Planck-Institut für Astrophysik

Master's Degree in Astrophysics

Master Thesis

Theoretische Vorhersagen zu den Oberflächenmagnetfeldern von binary-stripped, massereichen Sternen

Beutreuer

Prof. Dr. Selma E. de Mink

Jing-Ze Ma

Projektpartnerin

Prof. Dr. Ylva Götberg

Verfasser

Giovanni Stimamiglio

Sommer Semester 2025

Acknowledgments

First, I would like to thank my supervisor, Prof. Selma de Mink, for giving me the opportunity to work on this project and for always supporting me and guiding me throughout this thesis works as well as my first steps in the academic world.

I would also like to thank my daily advisor, Jing-Ze Ma, for his fundamental and continuous support, for all the time and discussions and, most importantly, for the invaluable help he gave me in shaping this project. Without him, I would not be as proud of how this thesis turned out as I am now.

I am grateful to Prof. Ylva Götberg for sharing her data and for all her help with the observational part of this work.

I would also like to thank all the wonderful people of the Stellar Group at MPA, who made me feel at home from day one.

Last but not least, I would like to thank, from the bottom of my heart, my family and my friends – Thibault, Bethany, Silvia, Ruggero, Amanda and all the others – without whom this would not have been possible.

ABSTRACT

Despite being extremely relevant in stellar evolution, the origin of magnetic fields of massive stars is still a major unresolved question. Surface magnetic fields have been detected in about 10% of massive stars, suggesting that internal fields could prove valuable in disclosing the riddle of massive star magnetism. Binary-stripped stars – stars that have lost their outer envelope due to interaction with a companion – present a natural laboratory to probe internal magnetic fields, as the removal of the envelope unveils stellar layers that are otherwise hidden. The recent discovery of the first observational sample of stripped He-stars provides a timely and unique opportunity to place direct constraints on internal magnetic fields in regions that were previously inaccessible, allowing for a direct comparison with theoretical models.

In this work, we aim to explore three different hypotheses for the origin of magnetic fields in massive stars: the fossil field scenario, where the field is inherited from star formation or stellar mergers; the convective core dynamo, in which the field is generated by convective motions within the core; and the rotational shear dynamo, where differential rotation between the core and envelope generates the field.

To achieve this, we use a detailed stellar evolution code to compute a numerical model of an intermediate-mass, binary-stripped He-star. After presenting the assumptions we make to calculate the field strength and evolution, we obtain a theoretical estimate of the field for each hypothesis. These estimates are then compared to the newly obtained observational upper limit in order to determine whether we can exclude any hypothesis.

In this work, we find that the convective core hypothesis, as we modeled it, can be excluded, since it predicts a field strength exceeding the observational upper limit. In contrast, the rotational shear hypothesis yields a field just below this limit, placing it on the verge of being constrained. For the fossil field, our model shows that a combined poloidal and toroidal field geometry is the most realistic, even if the obtained field value is below the observational upper limit, thus preventing us from excluding it a priori.

A stronger observational constraint is needed, as it would significantly improve our findings, some already approaching the current limit. In addition, it would serve as a strong motivation for more sophisticated modeling, for which this work provides a solid foundation. We therefore hope that our analysis will motivate the prioritization of observational time, as this would greatly aid in constraining these theories and improving our understanding of angular momentum transport in stars.

Contents

Acknowledgments iii

Layman Summary ix

Introduction 1

1 Observational constraints 3
- 1.1 Observational techniques for stellar magnetic fields . . . 3
- 1.2 Observational upper limit on the magnetic field from a binary-stripped star 6

2 Stellar models 9

3 Magnetic field evolution 11
- 3.1 Magnetic flux conservation . . . 11
- 3.2 Ohmic decay and magnetic buoyancy . . . 12

4 Quantitative predictions for three origin hypotheses 17
- 4.1 Fossil field hypothesis (I) . . . 17
- 4.2 Convective core hypothesis (II) . . . 21
- 4.3 Rotational shear hypothesis (III) . . . 23

5 Results and Implications 29

Conclusions 33

Bibliography 35

A Supplementary figures 41

Layman Summary

From the depths of outer space and the core of stars to our phone's chargers or headphones, magnetic fields can be found all around the Universe. In each of these aspects, they play a crucial role that is still often overlooked. But to understand why they are so central, we first need to ask: what is a magnetic field?

The Physics 101 definition is: "A magnetic field is an invisible force field generated by a magnet or as a consequence of the movement of electric charges."[1] Intuitively, it can be thought of as a special "map" that shows the strength and direction of the magnetic forces in every point around the generating source. The strength (or magnitude) of a magnetic field is measured in Tesla (T) in the International System of Units. However, in astrophysics, we usually work in Gauss (G), where $1\,\mathrm{G} = 10^{-4}\,\mathrm{T}$. Magnetic fields surround us, even if we don't always notice. They're essential to the functioning of electric motors and electronic devices, and they play a crucial role in medical technologies like MRI machines. Perhaps most importantly, Earth's magnetic field has helped and protected us since the dawn of time: guiding navigators with compasses, shielding us from cosmic radiation, and helping to keep our atmosphere in place.

In the Universe, magnetic fields are ubiquitous. They thread through galaxies, the interstellar medium and the interiors of stars, spanning several orders of magnitude in strength. Earth's field, for instance, is about 0.5 G. In the interstellar medium, it's a million times weaker, around 10^{-6} G, while on the surface of our own Sun it is around 1 G, with peaks of 4000 G in sunspots. On the opposite extreme, magnetars – some of the most magnetic objects in the Universe – can host fields as strong as 10^{15} G, which is fifteen orders of magnitude stronger than Earth's! To provide a familiar point of reference, a typical refrigerator magnet has a magnetic field strength on the order of 50 G. This is about 100 times stronger than Earth's field but remains negligible compared to the colossal fields found in magnetars. Even the most powerful magnetic fields ever generated in a laboratory, under very specialized conditions, only reach 4.52×10^5 G[2], very far from the astrophysical extremes.

In this thesis, we will investigate stellar magnetic fields, as they play a key role in shaping a star's behavior and evolution. They drive a plethora of surface phenomena – such as flares and spots – and they influence winds, thereby affecting how the star interacts with its surroundings.

In particular, we are interested in the fields of massive stars, which are stars at least eight times more massive than our Sun. Although they are less common than their smaller counterparts, their role in the Universe is fundamental. Their high mass leads to greater luminosity, but also shorter lifetimes as they consume their fuel in just a few million

[1] https://ec.europa.eu/health/scientific_committees/opinions_layman/en/electromagnetic-fields/glossary/mno/magnetic-field.htm

[2] J. Toth and S. T. Bole, "Design, Construction, and First Testing of a 41.5 T All-Resistive Magnet at the NHMFL in Tallahassee," in IEEE Transactions on Applied Superconductivity, vol. 28, no. 3, pp. 1-4, April 2018

years: they burn bright and fast. In their cores, massive stars forge the heavier elements of the Universe and, through their intense radiation and explosive deaths, shape their surroundings and drive galaxy evolution. The endpoints of their lives are neutron stars and black holes – the most compact objects in the Universe.

Magnetic fields of massive stars are especially important because they influence the internal rotation rate of the star and thus what happens when the star dies and becomes one of these compact objects. Strong magnetic fields can slow down a star's rotation before it collapses, affecting how fast the resulting remnant spins. Being able to predict how fast these remnants spin has important implications. For example, it allows us to compare with observations of black holes' spins coming from gravitational waves and electromagnetic signatures. Fast-spinning stellar cores are also believed to be the origin of magnetars and some of the most energetic events in the Universe such as gamma-ray bursts.

Nonetheless, the origin of massive star magnetism still poses a riddle. Less than a tenth of observed massive stars exhibit strong surface magnetic fields, while more are believed to host an internal field. Such field is, however, shielded by the envelope and thus out of our reach, as our best observational techniques only probe surface magnetism.

In this context, binary systems come to our rescue. These are pairs of stars that orbit a common center of mass and offer unique opportunities to study stellar properties. The more massive a star is, the more likely it is to be found in such a system. One of the most common outcomes of binary evolution is stripped stars, meaning stars that lost a major fraction of their outer envelope and are now basically exposed cores. How can this happen? As mentioned before, the bigger the star, the shorter its life: thus, the bigger star of the binary system – referred to as primary – will be the first to exhaust most the hydrogen in its core. As a result of this, the core contracts and outer layers of the star will begin to expand. If, in its expansions, the primary comes too close to its companion, some of its matter will fall under the secondary's gravitational attraction, getting pulled away and accreted – a mass transfer event has started. If the two stars are sufficiently close, this phase can last long enough for the secondary to accrete most of the primary's envelope, leaving behind a (binary-)stripped star.

For the magnetism of massive stars, this represents a unique opportunity to probe the internal magnetic field. The stripping leaves the inner layers exposed and allows us to apply the observational techniques for the surface fields. For a long time, however, binary-stripped stars with mass between two and eight times that of the Sun have evaded detection. This happens because they are often outshone by their companion, now extremely bright due to the newly accreted matter. Moreover, the bulk of the stripped star's light is emitted in the ultraviolet (UV) range, which is complicated to observe due to extinction. Extinction refers to the absorption and scattering of light by interstellar dust, which dims and reddens the starlight, especially at shorter wavelengths like UV. Very recently, a new sample of candidate binary-stripped star systems was observed, turning the tables and allowing us to infer a new preliminary upper limit for the magnetic field of one of such systems.

Such limit was inferred using spectroscopy – the study of spectra. The light coming from a star across different wavelengths is referred to as spectrum. Upon a closer look, a typical stellar spectrum is a collection of dark (absorption) or bright (emission) lines, generated by the interaction of photons with atoms, that cause electrons to move between energy levels. When a magnetic field is present, it interacts with the electrons causing the energy levels to split: where a single line was observed in absence of a field, now multiple closely spaced lines are visible. This is called Zeeman splitting, and it is the most direct consequence of the so-called Zeeman effect. Since the amount of splitting is directly proportional to the magnetic field strength, studying the spectra allows astronomers to

infer estimates of (surface) stellar fields.

In order to compare this new observational limit with theoretical estimates, we investigated three different scenarios. This approach stems from the uncertainty in the origin of the magnetic field of massive stars. The first origin hypothesis is the fossil field, which assumes that the field is inherited from star formation and is large-scale, meaning that it spans over the entire envelope of the star. The second and third hypotheses both involve a dynamo mechanism. A stellar dynamo is a process that generates and maintains a magnetic field via the motion of the star's electrically conducting plasma. This hot plasma moves inside a star due to either convection or rotation, creating electric currents that in turn generate magnetic fields. For the second hypothesis, we consider the dynamo caused by convective motions in the core. Convection is the process where hot material rises and cooler material sinks, creating circulating flows inside the star. This happens due to buoyancy, which is the same force that makes a ball, which is filled with air and thus less dense, rise when we try to push it underwater. On the other hand, the third hypothesis considers the dynamo generated by rotation, in particular rotational shear. The core and the envelope of a massive star rotate in the same direction but at different speeds – a process called differential rotation. This speed difference generates a shear layer that winds up the magnetic field, amplifying its azimuthal component.

After we define the theoretical basis for the three origin hypotheses, we apply them to a computational stellar model. We thus use a detailed stellar evolution code to simulate a binary system up until the stripped star phase. This code is one-dimensional, meaning that it assumes spherical symmetry and calculates the stellar properties only along the radius as if we were core-drilling the star from the surface down to its center. We then apply each origin hypothesis to the model, in order to obtain different theoretical estimates for the magnetic field strength. Our aim is to compare such estimates with the new observational upper limit, to determine whether any of them exceeds it. If a hypothesis predicts a field stronger than the observed limit, this would suggest that, under our approximations, it cannot possibly reproduce the observed field and can therefore be ruled out.

This represents another step towards a better understanding of massive stars' magnetism, which is extremely relevant in the evolution of these stars and is at the root of some of the most energetic and mysterious events of our Universe.

Introduction

Magnetic fields can be found all around the Universe, with magnitudes ranging from the ultra-strong fields of magnetars (up to 10^{15} G) down to the few μG of the interstellar medium. Due to their ubiquity, they hold a central role in every aspect of astrophysics, with stars being no exception. Magnetic fields permeate stellar structure and evolution in several aspects, from driving surface phenomena such as flares and spots (Reiners 2012) to influencing winds and the interaction with surrounding objects (Vidotto et al. 2009).

In particular, the interest in the magnetism of massive stars stems from their evolutionary fate as compact objects, either neutron stars (NS) or black holes: in both scenarios, the magnetic field strength before the collapse can heavily affect the spin of the remnant via magnetic braking (Mestel 1968; Bouvier et al. 2014) or angular momentum (AM) transport due to internal magnetic torques (Spruit 2002; Fuller et al. 2019). The latter is of particular interest, as the spin of the collapsing core plays a crucial role in determining the spin of the resulting compact remnant. Accurate knowledge of remnant rotation rates is valuable for numerous applications. For instance, comparing black hole spins inferred from stellar evolution models with those measured through gravitational wave observations (van der Sluys et al. 2008; Vitale et al. 2014; Baibhav et al. 2018) and electromagnetic signatures (Zhang et al. 1997; Reynolds & Fabian 2008; McClintock et al. 2011). Rapidly spinning stellar cores are also believed to be the progenitors of energetic transients such as gamma-ray bursts (GRBs), fast radio bursts (FRBs) and hypernovae (Duncan & Thompson 1992; Thompson et al. 2004). Furthermore, magnetars – neutron stars with extreme magnetic fields – are believed to originate from massive stars with magnetized, fast-spinning cores (Ferrario & Wickramasinghe 2006; Turolla et al. 2015).

However, detecting the magnetic fields of massive stars is very challenging. While low-mass stars ($\lesssim 1.1\,M_\odot$) exhibit surface magnetic fields believed to be generated by an ongoing dynamo in their convective envelope, only a small fraction ($\lesssim 10\%$) of intermediate- and high-mass stars show surface magnetism, according to observational surveys, e.g. the Magnetism in Massive Stars project (MiMeS, Wade et al. 2013, 2016). Nevertheless, since they host a convective core, the vast majority of massive stars are believed to host an internal magnetic field generated by a dynamo even if they don't exhibit a surface field. Yet, since our best observational tools only probe surface fields, this inner magnetism remains out of reach – concealed by the stellar envelope. Recently, with the rise of asteroseismology, we have been able to study the stellar interior through their pulsations (Aerts et al. 2010; Aerts 2021), allowing for a better understanding of their mixing and rotation profiles. However, its application to probing internal magnetic fields — an area known as magneto-asteroseismology (Bowman 2023) — has so far concentrated only on red giants (Deheuvels et al. 2023; Li et al. 2023), largely because asteroseismology of main sequence massive stars is far more challenging. This is due to larger oscillation periods and the influence on oscillations of various poorly understood physical phenomena (close binarity, fast rotation, mass loss) that happen in the outer layers of these stars (Aerts et al. 2010; Aerts 2014). The only exception is the pulsating main-sequence B-type star

HD 43317, for which a forward magnetic asteroseismic model exists, albeit with strong assumptions (Lecoanet et al. 2022).

In this context, binary systems emerge as a unique opportunity to probe the internal magnetism in massive stars. Approximately 70% of all massive stars are expected to interact with their binary companion during their evolution (Sana et al. 2012; Moe & Di Stefano 2017). According to theory, the most common outcome of this interaction is stripped stars, i.e. stars that lose their H-rich envelope to the companion via stable mass transfer or common envelope ejection. Binary-stripped stars are believed to be highly relevant to a variety of astrophysical processes. They are regarded, due to their high surface temperatures, as the origin of the hardest ionizing photons in stellar environments, possibly playing a role also in cosmic reionization (Saxena et al. 2020; Götberg et al. 2020). In addition, they are believed to be the progenitors not only of double-NS systems that will later result in gravitational wave events (Tauris et al. 2017), but also of H-poor core-collapse supernovae (Drout et al. 2011; Smith et al. 2011; Eldridge et al. 2013). In the context of magnetic fields in massive stars, binary-stripped stars represent a natural laboratory for investigating the nature and origin of their magnetism: internal fields that were previously hidden beneath the hydrogen envelope during the main sequence become exposed once the latter has been stripped via binary interaction, allowing for direct observations and comparison with theoretical models. However, in the intermediate mass range ($2 - 8\,M_{\odot}$), there has been a lack of observations of stripped star systems. This changed when a sample of candidate systems in the Magellanic Clouds was identified by Götberg et al. (2023) and Drout et al. (2023).

In this work, we test the three main origin hypotheses for the magnetic fields of massive stars through MESA (Modules for Experiments in Stellar Evolution, Paxton et al. 2011, 2013, 2015, 2018, 2019; Jermyn et al. 2023) models of a binary-stripped He star system, that we then compare with an observational upper limit obtained from the sample of Götberg et al. (2023). The hypotheses are: (I) fossil field (Spitzer 1958; Mestel 1965), (II) convective core dynamo (Parker 1979; Moss 1989; Charbonneau & MacGregor 2001; Augustson et al. 2016) and (III) rotational shear dynamo (Spruit 2002; Fuller et al. 2019). We find that the field predicted by the fossil field hypothesis is highly influenced by the choice of geometry and initial magnitude; on the contrary, the convective core hypothesis, under our assumptions, yields a field above the observational upper limit and can therefore be excluded, while the rotation shear hypothesis results in a field below the observational threshold, preventing us from excluding it a priori. Overall, although some scenarios can be excluded under our approximations, a better constraint on the observational limit for the field could largely improve our results, allowing for a better understanding of the origin of magnetism in massive stars.

In Sect. 1, after a brief overview of the main observational techniques, we present the upper limit derived from observations and in Sect. 2 we introduce the numerical setup of our simulations. In Sect. 3 we present the main assumptions adopted, while in Sect. 4 we investigate in detail each origin hypothesis for the magnetic field. Our results and their implications are discussed in Sect. 5.

Chapter 1

Observational constraints

Motivated by the recent discovery of a sample of binary-stripped He-stars by Götberg et al. (2023) and Drout et al. (2023), in this work we provide theoretical estimates of the magnetic field of a massive star in such a system. We then compare our findings with a newly derived observational upper limit inferred from one of the stars in the sample. To this end, the present chapter offers a brief overview of the main observational techniques used to detect stellar magnetic fields – both at the surface and in the stellar interior – followed by a presentation of the new observational constraint.

REST IS TBD.

1.1 Observational techniques for stellar magnetic fields

The detection of surface magnetic fields in stars relies on the Zeeman effect. As originally observed by Zeeman (1896), spectral lines appear to broaden in the presence of an external magnetic field. Through quantum mechanics, we now understand that this broadening is caused by the change in the potential energy levels due to a (static) field. A schematic representation can be seen in Fig. 1.1

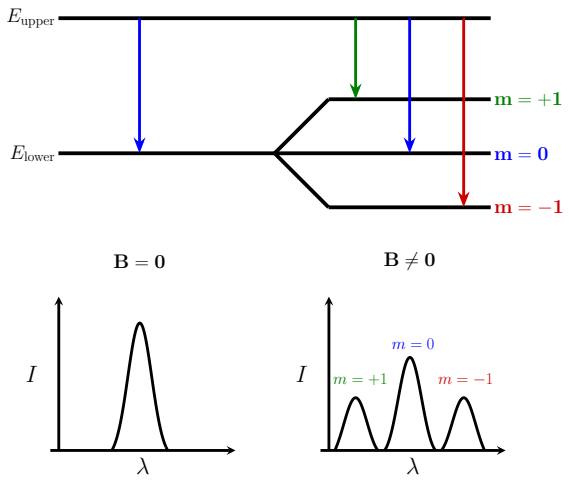

Figure 1.1: Schematic representation of the Zeeman effect. We show how the energy level split in the presence of a magnetic field and, in the lower part, the resulting intensity line profiles. The figure shows a triplet, where the energy level splits into three components. In general, the number of sub-levels in a multiplet depends on the quantum number of the energy level.

The potential energy levels are modified according to

$$U = m\mu_b B\,, \tag{1.1}$$

where m is the magnetic orbital quantum number, μ_b is the Bohr Magneton and B the external magnetic field. For a strong enough field, the broadening increases to a point where the line splits due to multiple energy levels becoming available for a transition. The effect on the spectra is the creation of multiple lines. Thus, line splitting in stellar spectra is a clear indicator of the presence of a surface magnetic field and allows for an estimate of the field strength.

While the line splitting is observed in the spectra, and thus in the total intensity of the incoming radiation, Zeeman effect also plays a role in the polarization of the light. Generally, light coming from a star is unpolarized, meaning that it's the sum of randomly polarized components. However, interaction with an external magnetic field causes light to be mainly circularly polarized. To better understand this, we rely on the Stokes vector $[I, Q, U, V]$, which is commonly used to mathematically describe light and its polarization (Stokes 1851; Chandrasekhar 1960):

- Stokes I is the total intensity of the radiation, i.e. what is typically recorded in spectroscopy;
- Stokes Q and U give the amount of light that is linearly polarized, either vertically/horizontally (Q) or at 45° (U);
- Stokes V gives the amount of light that is left- or right-handed circularly polarized.

For the Zeeman effect, the different components of the transition will have different polarization states. In particular, the longitudinal component of the field – that is the component along the line-of-sight – will circularly polarize the transitions with $\delta m = \pm 1$ (Landstreet 2009). Since $V = m_1 - m_{-1}$, Zeeman effect will result in $V \neq 0$ and thus circularly polarized light coming from the star. The study of the polarization of the spectra coming from a star is referred to as spectropolarimetry, and it can be used to infer the magnetic field (Landstreet 2014). A comparison of how a magnetic field affects the Stokes I and V parameters can be found in Fig. 1.2

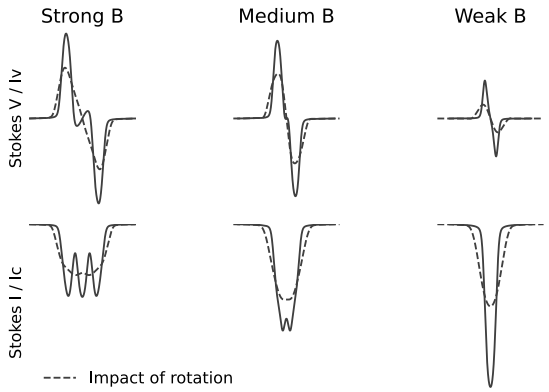

Figure 1.2: Illustration of the impact of rotation and dipolar field strength on the Stokes I and V line profiles. From Petit & Oksala (2025).

Other effects, such as thermal motions or rotation (as shown in Fig. 1.2), lead to broadening of the lines, thus a precise analysis and a good resolution are needed to infer the star's magnetic field from the spectra. Spectroscopy allows for the inference of the mean field strength averaged over the stellar disk ($\langle|\mathbf{B}|\rangle$) from the splitting of the Stokes I

parameter. On the other hand, spectropolarimetry probes the longitudinal component of the field only (B_ℓ) that affects the Stokes V parameter.

These techniques are widely used to detect the surface magnetic field of stars across the Hertzsprung-Russel diagram. For single massive stars, the MiMeS survey (Wade et al. 2013) and the BOB Collaboration (Schöller et al. 2017) employed these techniques to compile an extensive catalog of magnetic massive stars. Spectropolarimetry has also been used to detect fields in binary stars (Grunhut et al. 2012).

Probing the internal magnetic field of stars is more challenging. Only recently the rise of asteroseismology disclosed the possibility of studying stellar interiors (Aerts et al. 2010; Aerts 2021). The application of asteroseismology to probe internal stellar magnetic fields – known as magneto-asteroseismology (Bowman 2023) – is still in its early stages. This is largely because, although the theoretical impact of magnetic fields on stellar oscillations has been recognized for decades (Gough & Thompson 1990; Hasan et al. 2005), observational evidence has only recently become widely available. To date, the primary focus has been on red giants, whose oscillations allow for the inference of internal magnetic fields primarily through three seismic signatures.

The first signature is dipolar mode suppression. Red giants exhibit mixed-modes, which are oscillations that behave as gravity waves (g-modes) near the core and pressure waves (p-modes) closer to the surface (Scuflaire 1974; Osaki 1975; Aizenman et al. 1977; Unno et al. 1989; Dziembowski et al. 2001). Approximately 20% of red giants exhibit an abnormally lower amplitude of the dipolar mixed-modes (Mosser et al. 2012; García et al. 2014; Stello et al. 2016). To explain this phenomenon, the so-called "magnetic greenhouse effect" was proposed: if the magnetic field around the core surpasses a critical strength (B_c), magneto-gravity waves can no longer propagate and are trapped or disrupted (Fuller et al. 2015; Stello et al. 2016; Rui & Fuller 2023). Dipolar modes are the most affected, causing the suppression exhibited by observations. Careful modeling of the observed suppression allows for the inference of the critical field in the core or near-core region.

Another possibility is asymmetries in rotational multiplets. The degeneracy of oscillation modes of red giants can be broken by both rotation and magnetic fields. This generates modes with the same degree l, but different azimuthal order m, that are referred to as multiplets (e.g., for $l = 1$ it will be a triplet with $m = 0, \pm 1$). When the rotation rate is moderate, it generally produces multiplets symmetric with respect to the central $m = 0$ component. However, multiple studies have shown that the addition of magnetic fields will break the symmetry of these rotational multiplets (Deheuvels et al. 2017; Gomes & Lopes 2020; Mathis et al. 2021; Bugnet et al. 2021; Loi 2021; Mathis & Bugnet 2023). This effect has been demonstrated observationally by Li et al. (2022, 2023), who were able to infer the magnetic field strength from the observed asymmetry.

The last signature is period-spacing deviation. Bugnet (2022) demonstrated that the presence of stable internal magnetic fields in a red giant generates a bias towards lower values in the estimates of g-mode period-spacing. Thus, understanding how the period-spacing is affected by the internal field can yield estimates of the strength of said field.

However, these techniques have only been applied to red giants, also because of the complexity in understanding massive stars' oscillations. This is mainly due to the influence on oscillations of various poorly understood physical phenomena (close binarity, fast rotation, mass loss) that happen in the outer layers of these stars (Aerts et al. 2010; Aerts 2014; Bowman 2020, 2023). The only massive star for which a magneto-asteroseismic model exists is the pulsating B-type main sequence star HD 43317. Using the best-fitting model of Buysschaert et al. (2018), Lecoanet et al. (2022) were able to constrain an upper limit of the near-core field of this star assuming a dipolar field and a rigid rotation profile. Nevertheless, the application of magneto-asteroseismology to massive stars remains

a developing field, with very limited observational data currently available.

1.2 Observational upper limit on the magnetic field from a binary-stripped star

Binary stars offer a unique opportunity to probe the internal magnetic fields of massive stars, as a common outcome of binary interaction is stripped stars, i.e. stars that are stripped of their hydrogen-rich envelope. Without the envelope, the internal field becomes exposed and can be detected using the techniques for surface fields presented in the previous section.

However, observational data on binary-stripped helium stars in the intermediate-mass range ($2-8\,M_\odot$) have been notably scarce, with only a single candidate system previously proposed (Groh et al. 2008). This situation has changed very recently, with the discovery of a new sample of candidate systems in the Magellanic Clouds by Drout et al. (2023) and Götberg et al. (2023). In particular, eight systems from this sample have been classified as 'Class 1' or 'Helium-star Type', based on the fact that their optical spectra are dominated (by more than 80%) by the helium star component. The influence of the companion in the optical flux of these systems is thus small enough to allow for magnetic field inference from the optical spectra using Zeeman splitting.

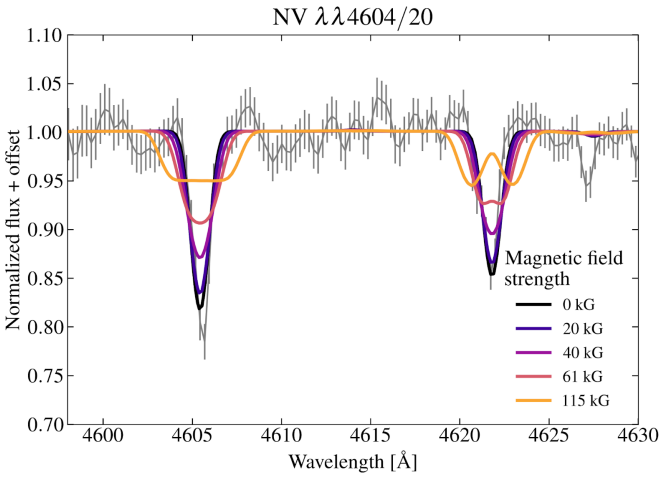

Figure 1.3: Zeeman broadening due to different field strengths on the NV 4604/20 lines. In gray, the observed spectrum of star 6 of Götberg et al. (2023). The overplotted colored lines represent the effect on the lines of a magnetic field of increasing intensity calculated through a model that accounts for the Zeeman effect. Credits: Ylva Götberg.

To infer the magnetic field strength, we compare the observed spectra with the model one accounting for Zeeman splitting. In Fig. 1.3 we apply different magnetic field strengths to the NV 4604,20 lines of star 6 of the sample of Götberg et al. (2023). It is clear how the observed spectrum (in gray) does not show any splitting. Thus, we can confidently rule out any field above 100 kG, since at that field strength the model starts to exhibit splitting in the NV 4620 line. From the line width, we can further derive a reasonable observational upper limit on the magnetic field strength of

$$B_{\mathrm{max,CHeB}} \simeq 50\,\mathrm{kG}\,. \tag{1.2}$$

Line depth cannot be reliably used, as it may be influenced by factors such as temperature or nitrogen abundance. In contrast, the line shape is more distinctive and can therefore be used to constrain the magnetic field strength.

We emphasize that this constitutes a preliminary estimate and that more comprehensive modeling, along with improved observational data, will be necessary to derive a more robust constraint.

Chapter 2

Stellar models

To obtain numerical estimates on the field strength for the different origin hypotheses, we construct stellar models using the 1D stellar evolution code MESA (Modules for Experiments in Stellar Evolution, release 23.05.1, Paxton et al. 2011, 2013, 2015, 2018, 2019; Jermyn et al. 2023) to evolve a binary system from the zero-age main-sequence (ZAMS) to He core depletion. The models' initial parameters are chosen to reproduce the observed properties of star 6 of Götberg et al. (2023) and Drout et al. (2023) after the stripping: at ZAMS the primary star has $M_1 = 11\,M_\odot$ while the secondary is a point mass of $M_2 = 9\,M_\odot$. A comparison between the main parameters of the system from the observations and from the model can be found in Table 2.1. The choice to use a point mass for the companion stems from the main focus of our work, which is the magnetic field of the primary star. Moreover, this approximation is reasonable, since for the system chosen the stripped star dominates the observed spectra (contributing for more than 80%, Drout et al. 2023), drastically reducing the influence of the secondary. The initial metallicity of the primary is $Z = 0.006$, which is appropriate for the LMC, and the stars are orbiting with an initial period of $P_{\rm ini} = 20$ days. The convective regions are calculated using the mixing-length-theory (MLT) with $\alpha_{\rm MLT} = 2.0$, and their boundaries are determined following the Ledoux criterion. The mass loss due to wind follows the Dutch scheme implemented in MESA (Glebbeek et al. 2009). The models for the field at main-sequence and convective core hypotheses are non-rotating, while the model for the rotational shear hypothesis has an initial surface rotation speed of $v_{\rm init} = 150\,{\rm km/s}$.

In Fig. 2.1 we show the evolution of the primary star of our non-rotating model, with the main phases identified by colored pluses. After its evolution along the main-sequence, the primary star will end its core H-burning phase and leave the main-sequence where the characteristic hook feature is (terminal-age main-sequence, TAMS) and its envelope will start expanding in the Hertzsprung gap. In this phase, the star fills its Roche lobe and a case B mass transfer event, where mass transfer begins after hydrogen core exhaustion (Kippenhahn & Weigert 1967; de Mink et al. 2008), starts, with the primary being stripped of most of its envelope. After regaining equilibrium, the star starts core He-burning (from now on, CHeB stage), becoming a stripped He-star: we follow its evolution up until core He depletion. All the results presented in this work are calculated at CHeB since at that stage the star is stripped and long-lived.

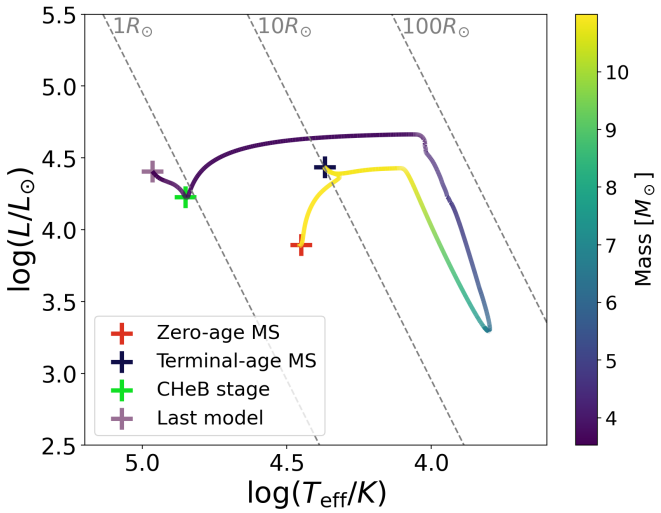

Figure 2.1: Hertzsprung–Russell diagram of the primary star for the non-rotating model. The colored pluses locate the main phases of the evolution of the star: zero-age main-sequence (green), terminal-age main-sequence (yellow), core He-burning stage (purple) and core He depletion (red). The gray dashed lines indicate constant radii. The colorbar indicates the mass of the star during its evolution.

Parameter	Observations	MESA model [at CHeB]	Comparison
M $[M_\odot]$	3.7 ± 0.9	3.6	Good agreement ($< 1\sigma$)
$T_{\rm eff}$ [K]	$7.3^{+1.4}_{-1.6} \times 10^4$	7.1×10^4	Good agreement ($< 1\sigma$)
$\log_{10}(g/[\rm cm/s])$	5.0 ± 0.3	5.1	Good agreement ($< 1\sigma$)
$X_{\rm H,surf}$	$0.35^{+0.20}_{-0.15}$	0.29	Good agreement ($< 1\sigma$)
$\log_{10}(L/L_\odot)$	$4.2^{+0.2}_{-0.3}$	4.2	Good agreement ($< 1\sigma$)
$R_{\rm eff}$ $[R_\odot]$	$0.81^{+0.09}_{-0.06}$	0.86	Good agreement ($< 1\sigma$)

Table 2.1: Comparison between the main system parameters of the observations (Star 6 of Götberg et al. 2023 and Drout et al. 2023) and the MESA model used in this work. From top to bottom, the parameters are the the stripped He-star's total mass (M), effective temperature ($T_{\rm eff}$), effective gravity (g), surface hydrogen fraction ($X_{\rm H,surf}$), luminosity (L) and effective radius ($R_{\rm eff}$).

Chapter 3

Magnetic field evolution

3.1 Magnetic flux conservation

Here we introduce a fundamental assumption that we will use throughout this work: magnetic flux conservation (Alfvén 1942; Braithwaite & Spruit 2017; Keszthelyi 2023). This means that as the star's surface area changes (e.g. during expansion or contraction), its surface magnetic field adjusts inversely to keep the total magnetic flux constant.

First, we define the magnetic flux Φ due to a field $\mathbf{B}$ at a given Lagrangian mass coordinate m as the integral of the field over a closed surface area $\mathbf{\Sigma}$:

$$\Phi = \oint_{\Sigma} \mathbf{B} d\mathbf{\Sigma} \simeq 4\pi R(m)^2 B \,, \tag{3.1}$$

where, due to spherical symmetry, we have calculated the surface area as a sphere of radius $R(m)$ and B is the radial component of the magnetic field averaged over this shell. Assuming that the flux is conserved means that the above expression needs to be constant over time, i.e.

$$\frac{\partial \Phi}{\partial t} = 0 \,. \tag{3.2}$$

This implies that, introducing a time dependence in equation 3.1, we expect

$$\Phi(t) = \Phi(t') \implies 4\pi R(m,t)^2 B(t) = 4\pi R(m,t')^2 B(t') \,, \tag{3.3}$$

for $t' > t$. The radius was expressed as a function of both the Lagrangian mass coordinate and time to reflect the evolving stellar structure. As the star expands or contracts during its evolution, the radial position associated with a given mass coordinate changes over time; that is, $R(m,t) \neq R(m,t')$. This can clearly be seen in Fig. 3.1, that shows the evolution of the radial coordinate at a given mass shell as a function of time.

Rearranging Eq. 3.3 to calculate the field strength at t' for a fixed mass coordinate m gives

$$B(t') = B(t) \left(\frac{R(t)}{R(t')} \right)^2 . \tag{3.4}$$

In the following, we refer to the term in the parenthesis on the left as the amplification factor: it is relevant since it is hypotheses-independent, meaning that its value remains the same regardless of the field origin as it purely depends on the change in the star's structure. It also expresses how the field strength at a given mass shell changes due to the evolution of the star itself: if over time the mass shell contracts, the field is amplified and vice versa. Thus, if during the main-sequence a magnetic field was already present

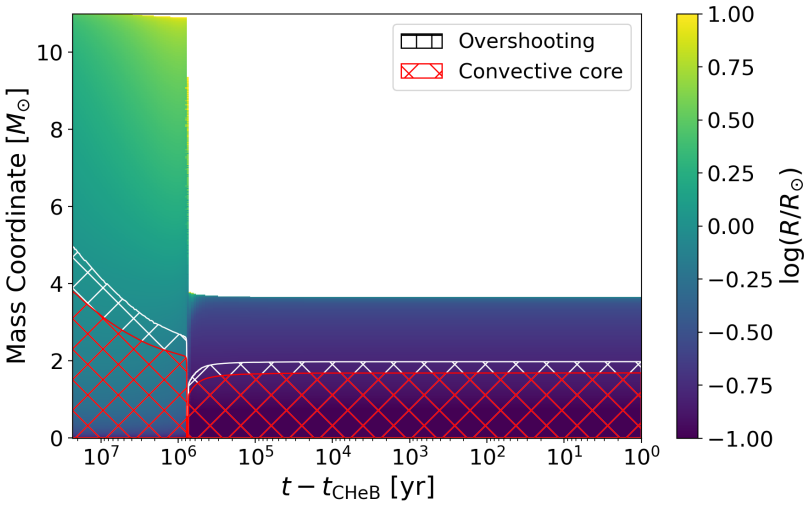

Figure 3.1: Kippenhahn diagram showing the evolution of the radial coordinate at each mass shell. The colorbar shows the logarithm of the radius. The red hatched region indicates the convective core, while the white one the overshooting layer.

in the shell corresponding to the surface of the stripped star, this amplification factor will influence the field strength at CHeB. As we will see, this is the case for the fossil field and convective core dynamo hypotheses.

3.2 Ohmic decay and magnetic buoyancy

For the convective core hypothesis, we will assume that a field generated in a convective region will remain "frozen" in the radiative layers left behind by core retreat. This means that, when the core retreats during the main-sequence, any mass shell that ever hosted a dynamo will retain the field it had the last time it was convective. A more thorough discussion of this approximation can be found in Sect. 4.2.

To test the validity of this approximation, we investigate one way to destroy the frozen-in magnetic field: Ohmic decay, which is the decay of the field due to magnetic diffusion. In this section, we show that Ohmic decay is a very slow process that only has limited effects on the magnetic fields of massive stars. This can be inferred by calculating the Ohmic timescale, which defines the time a field in a radiative layer takes to diffuse across a pressure scale height H_P:

$$\tau_{\mathrm{Ohm}} = \frac{H_P^2}{\eta}\,, \tag{3.5}$$

where η is the magnetic diffusivity (i.e. the inverse of the electrical conductivity). In this work, we are interested in observing the field at CHeB stage, i.e. after the stripping has happened. This is the case if, during the main-sequence, the Ohmic timescale is bigger than the main-sequence lifetime of the star (estimated by the nuclear timescale $\tau_{\mathrm{nuc,H}}$). In addition, the field can be detected at CHeB only if it is long-lived against Ohmic diffusion for the whole He-burning lifetime, meaning $\tau_{\mathrm{Ohm}} > \tau_{\mathrm{nuc,He}}$.

Thus, we calculate the evolution of the Ohmic timescale at the mass shell of the surface of the stripped star, to assess if the frozen field would be long-lived against Ohmic diffusion. The evaluation of the magnetic diffusivity in stellar matter is rather tricky, as the formula depends on the degeneracy of stellar matter. From direct calculation of the degeneracy parameter, that is shown in Fig. 3.2, it is clear how, for our model, the matter is non-degenerate. Thus, we calculate η by incorporating into MESA the definitions from Spitzer

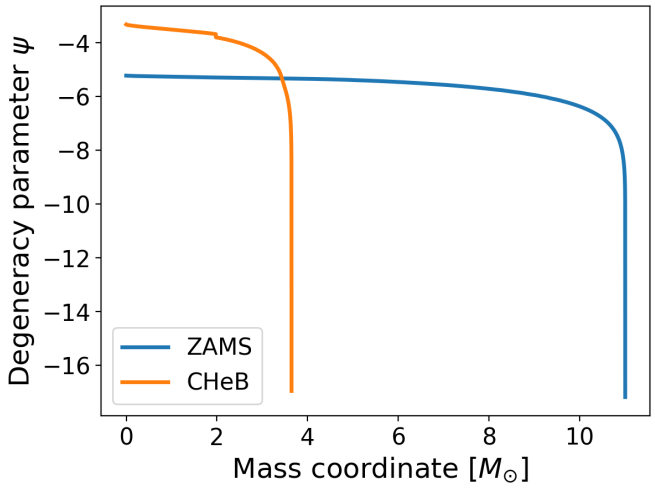

Figure 3.2: Profile plot of the degeneracy parameter, showing the behavior of the latter as a function of mass shell at ZAMS (blue line) and at CHeB stage (orange line).

(1962) and Wendell et al. (1987). Given that the magnetic diffusivity is the inverse of the electrical conductivity σ ($\eta = 1/\sigma$) we define for the low-temperature, high-density regime

$$\sigma = \gamma_E \frac{2(2kT)^{3/2}}{\pi^{3/2} m_e^{1/2} Ze^2 \ln(\Lambda + 1)}\,, \tag{3.6}$$

where k is the Boltzmann constant, T the temperature, m_e the electron mass, Z the ion charge number and e the electron charge. The correction factor for e-e scattering (γ_E) is $\gamma_E = 0.582$ for hydrogen, while $\gamma_E = 0.683$ for He (as in Table 5.4 in Spitzer 1962). The value for Λ is defined as

$$\Lambda = \frac{3}{2Ze^3} \frac{(kT)^{3/2}}{(\pi n_e)^{1/2}} \times \begin{cases} 1\,, & \text{for } T < T_0\,; \\ \left(\frac{T_0}{T}\right)^{1/2}\,, & \text{for } T \geq T_0\,, \end{cases} \tag{3.7}$$

where $T_0 = 4\alpha^2 c^2 m_e / 3k$, for α the fine structure constant and c the speed of light. The results for the Ohmic timescale can be seen in the top panel of Fig. 3.3.

During the entire main-sequence, between the two dashed lines that respectively represent the temporal location of the ZAMS and the TAMS, we find $\tau_{\rm Ohm} \sim 10^{12}$ yr, that is much bigger than the nuclear timescale $\tau_{\rm nuc,H} = 1.4 \times 10^7$ yr: thus, the field will survive up until the stripping. However, we notice a very steep decrease in the Ohmic timescale as we approach CHeB stage at the endpoint of the graph, which corresponds to when that mass shell arrives at the surface of the star after the stripping. To investigate this feature, we calculate $\tau_{\rm Ohm}$ for each mass coordinate at CHeB: the results are shown in the bottom panel of Fig. 3.3. It can be clearly seen how, in the deeper layers of the star, the Ohmic timescale is much bigger than the nuclear timescale $\tau_{\rm nuc,He} \simeq 2.2 \times 10^6$ yr, while a steep decrease can be observed only at the very surface. This drop is caused by the increase of the magnetic diffusivity and the simultaneous large decrease in the pressure scale height as we approach the surface. These behaviors can be explained by the temperature dependence of both η and H_P near the surface. In the interior layers, pressure scale height also represents the magnetic field length scale ($H_P \simeq H_B$, Cantiello & Braithwaite 2011): thus, the dropping value of H_P close to the surface is a problem as the field geometry is not expected to change in those layers. Therefore, it is reasonable to assume that close to the surface $H_P \neq H_B$, especially since the field is not generated in these layers. Nevertheless, in order to provide a more conservative field estimate, we

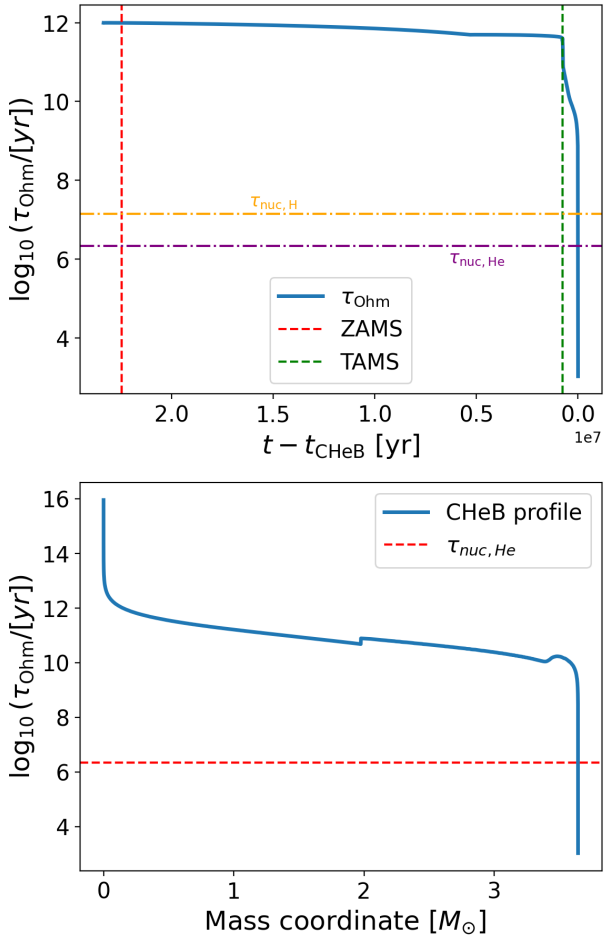

Figure 3.3: (Top panel) Time evolution of the Ohmic timescale at the Lagrangian mass coordinate of the surface of the stripped star. The vertical dashed lines show the time coordinates of the ZAMS and TAMS respectively. (Bottom panel) Profile plot of the Ohmic timescale as a function of mass coordinate at CHeB. The step-like feature at a mass coordinate of around 2 is due to the presence of the core/envelope limit, which generates a bump in both the values of the pressure scale height and of the magnetic diffusivity. The horizontal red dashed line shows the He nuclear timescale.

further investigate the near-surface layers to see how the field changes where the ohmic timescale is comparable to the nuclear one: we find that the difference in mass between the surface and the first mass coordinate at which $\tau_{\rm Ohm} > \tau_{\rm nuc,He}$ is $\Delta m = 10^{-6}\,M_\odot$, that is 10^{-7} of the total mass of the star. Mass-wise this difference is negligible, but if we calculate the same difference in the radial coordinate, we find $\Delta r = 5.0 \times 10^{-2}\,R_\odot$, corresponding to roughly 5.85% of the total radius, that is a non-negligible difference. Thus, to find such a field at the surface of the stripped star, we need to investigate the timescales of possible mechanisms that could bring to the surface the field located in the first stable mass coordinate.

The first process that may play a role is mass loss: massive stars have a high mass loss rate, which implies that material residing on the surface will remain there for a short time. We calculate the mass-loss timescale as

$$\tau_{\dot{M}} = \frac{\Delta m}{\dot{M}_{\rm rate}}\,, \tag{3.8}$$

where Δm is the mass difference between the surface and the first mass coordinate at which $\tau_{\rm Ohm} > \tau_{\rm nuc,He}$ and $\dot{M}_{rate}$ is the mass loss rate of the star. We find $\tau_{\dot{M}} = 7.6$ yr, which is much smaller than all relevant timescales for the star.

Another possible way to bring the field to the surface is represented by magnetic buoyancy, as originally proposed by Parker (1955). We consider a self-contained magnetic feature of size l inside the radiative layers of the star. From hydrostatic equilibrium, the feature needs to be in pressure equilibrium with the surroundings:

$$p_e = p_{\rm mag} + p_i \tag{3.9}$$

where $p_{\rm mag} = B^2/24\pi$ is the magnetic pressure of the feature, while $p_e\,, p_i$ are respectively the total (gas+radiation) pressures outside and inside the feature. Since we always have $p_{mag} > 0$, the pressure condition implies $p_e > p_i$ that, assuming thermal equilibrium between the feature and the surroundings $T_e = T_i$, yields $\rho_e > \rho_i$, causing the feature to rise. The speed of said rise depends on the importance of thermal diffusion, which is controlled by the value of the thermal diffusivity:

$$\chi = \frac{4acT^3}{3\rho^2 c_p \kappa}\,, \tag{3.10}$$

where T and ρ are the temperature and the density at a given mass coordinate, a is the radiation constant, c_p is the specific heat at constant pressure and κ is the Rosseland mean opacity. If there is no thermal diffusion, no heat exchange can happen between the surroundings and the feature: the latter will thus rise due to the density difference up until it reaches an equilibrium where $\rho_e = \rho_i$, which implies $T_i < T_e$. Instead, accounting for small thermal diffusion, the difference in temperature triggers heat exchange, with the feature absorbing heat from the surroundings and thus rising quasistatically upwards with speed (MacGregor & Cassinelli 2003; Hansen et al. 2004; Cantiello & Braithwaite 2011):

$$v_{\rm therm} \simeq \frac{2\chi H_P}{l^2 \beta(\nabla_{ad} - \nabla)} \frac{1}{4 - 3\alpha}\,, \tag{3.11}$$

where $\beta = P_e/P_{mag}$, $\alpha = P_{\rm gas}/P_{\rm tot}$, while ∇ and ∇_{ad} have the usual definitions.

On the other hand, if the thermal diffusion is large, the heat exchange happens very fast and in good approximation we have $T_e = T_i$: thus, the density equilibrium condition cannot be fulfilled and the feature rises due to the density difference $\rho_e > \rho_i$ so fast that its speed is limited by aerodynamic drag. By equating the buoyant force (given by Archimedes' principle) to the drag force we can thus obtain an equation for the drag-limited rise speed:

$$\frac{1}{2} C_d A \rho_e v_{\rm drag}^2 = V g \Delta\rho \quad \Longrightarrow \quad v_{\rm drag}^2 \approx \left(\frac{2V}{C_d H_P A}\right) \frac{P_{mag}}{\rho_e}\,, \tag{3.12}$$

where C_d is the drag coefficient, A and V are the cross-sectional area and volume of the feature and $\Delta\rho = \rho_e - \rho_i$, that in this regime is non zero. Given that $l \approx V/A$, the bracketed term can be rewritten as l/H_P, while the rest is approximately the Alfvén speed that, expressed as a function of the sound speed c_s and β, yields

$$v_{\rm drag} \sim \frac{c_s}{\sqrt{\beta}} \sqrt{\frac{l}{H_P}}. \tag{3.13}$$

We thus applied these formulas to our convective dynamo model, to calculate the buoyancy timescales in the two regimes (subscripts s and l respectively for the small and large thermal diffusion limits) as

$$\tau_{\rm buoy,s} = \frac{H_P}{v_{\rm therm}}\,; \qquad \tau_{\rm buoy,l} = \frac{H_P}{v_{\rm drag}}\,. \tag{3.14}$$

To complete the calculation, we thus need to assign a value to the two parameters that do not directly come from the simulation, namely l and β. We adopt the conservative estimate $l \approx H_P$ and $\beta \approx 100$: for the first, the choice stems from the most probable size of the magnetic feature in the radiative layer (Cantiello & Braithwaite 2011); on the other hand, from direct calculation $\beta \sim 30$ in the subsurface layer we are considering (see Fig. A.1 in Appendix A), thus the value chosen is a conservative estimate given the fast variability shown by the parameter. A magnetic feature with said characteristics shows $\tau_{buoy,s} = 6.13$ h and $\tau_{buoy,l} = 0.15$ h, which are much shorter than any other timescale for the field's rise. Direct calculation of the thermal diffusivity of Eq. 3.10 in the relevant subsurface layer points to the high χ regime as the preferred one, but in both cases the buoyancy timescale is short enough to guarantee, in good approximation, that the surface field with $\tau_{\rm Ohm} < \tau_N$ gets continuously replaced by a lower-layer field long-lived against Ohmic diffusion and thus detectable.

Chapter 4

Quantitative predictions for three origin hypotheses

The origin of magnetic fields in massive stars is debated. In most reviews on stellar magnetism (e.g. Walder et al. 2012; Braithwaite & Spruit 2017; Augustson 2019; Keszthelyi 2023), two main origin hypotheses are presented: the fossil field and the dynamo scenarios. Both cases aim to explain the incidence and strength of magnetic fields observed among massive stars, thus focusing on understanding and reproducing surface fields. However, as mentioned in the previous sections, binary-stripped stars represent a unique opportunity to study internal fields of massive stars, without the need for them to rise to the surface to be detectable. In this work, we present a slightly different classification of the origin hypotheses, as follows:

I. Fossil field hypothesis, equivalent of the homonymous scenario in classical reviews, in which a large-scale, ordered magnetic field is present during the main-sequence both in the interior and on the surface. The origin of such field may vary and will be investigated in the dedicated section;

II. Convective core dynamo hypothesis, in which the magnetic field is generated inside the convective core of the star via a dynamo;

III. Rotational shear dynamo hypothesis, in which the field is generated in the radiative layer between the core and the envelope via a dynamo fueled by the differential rotation.

Hence, while the first classical scenario is investigated in the first hypothesis, in this work we will divide the dynamo scenario in two, making a distinction between dynamos operating respectively in the convective and radiative layers of the star. The last two hypotheses thus consider the presence of an only internal field during the main sequence, that is later exposed to the surface via binary-stripping.

4.1 Fossil field hypothesis (I)

In the fossil field hypothesis, we assume the presence of an ordered, large-scale magnetic field already during the main-sequence, both on the surface and in the internal layers of the star. The origin of such a field is not clearly defined, with several proposed possibilities. In the following, we give a brief overview of the most accredited hypotheses.

In the first proposed origin scenario, the fossil field is inherited from star formation (Tout et al. 2004; Ferrario & Wickramasinghe 2006): if the molecular cloud from which a

star originated is magnetized, the collapse will greatly amplify the magnetic field if flux conservation is assumed. However, the amount of flux actually accreted onto the star is not clearly defined, as it has been calculated that total accretion coupled with "pure" flux conservation would lead to a too high amount of flux being retained by the star (for example, Braithwaite (2012) proposes MHD instability and buoyant expulsion as ways to destroy flux accreted by the protostar).

Another possibility is that the field is the result of a merger event, during which the (weak) field of one of the components gets greatly amplified (Schneider et al. 2019). For example, this mechanism could explain the magnetic tertiary in the triple system as as observed by Hubrig et al. (2025). A merger in the pre-main-sequence or in the early stages of evolution would lead to a magnetized star applicable to our case: Wang et al. (2022) showed that early mergers could explain the blue main-sequence band in young clusters and the bi-modality in magnetic fields. However, to be a viable candidate in our case, such a merger would need to occur in a triple system that later shrinks, allowing mass transfer to take place during the Hertzsprung gap. Thus, the parameter space would be limited and thus the applicability to our case would need further investigation that is beyond the scope of this work.

Lastly, the field could be generated by pre-main-sequence convection via a dynamo: massive stars in the pre-MS stages are fully convective, thus a convective dynamo will generate a field in this phase (Braithwaite & Spruit 2017). However, it is unclear whether this field would survive to be detectable during the main-sequence.

Since we are interested in the field at the surface of the stripped star, it is beyond the scope of this work to further investigate these possibilities: in this section we will assume the presence of a field in the main-sequence, not considering how such field originated. Instead, what is relevant is the geometry of said field. As a starting point, we assume that the large-scale field follows a poloidal configuration (with a radial component but no azimuthal component) of equation:

$$B(r) = \mu_B r^{-x}\,, \tag{4.1}$$

where the magnetic moment is defined as $\mu_B = B_{\rm surf,ZAMS} R^x_{\rm surf,ZAMS}$. Here, $B_{\rm surf,ZAMS}$ is the surface field strength at ZAMS, and $R_{\rm surf,ZAMS}$ is the radius of the star at ZAMS. The initial field value is a free parameter that strongly influences our results. The other free parameter is the exponent of the radial dependence x that radically changes the filed geometry. Thus, to quantify the effects of the choice of said parameters, we perform the analysis for a series of possible values. For the initial field strength $B_{\rm surf,ZAMS}$, as a lower value we choose 10 G, while as an upper value we use 75 kG: this range resembles the limits of the observational sample of magnetized B-type stars compiled by Makarenko et al. (2021), that includes stars mainly from the MiMeS (Wade et al. 2013) survey and the BOB Collaboration (Schöller et al. 2017). For the x parameter, we investigate the range between a lower value of $x = 0$ (uniform field) and $x = 6$ (steep radial dependence), focusing in particular on the dipolar configuration $x = 3$, that is the simplest form of a poloidal field.

First, we use Eq. 4.1 to calculate the field strength at ZAMS at the radius corresponding to the Lagrangian mass coordinate of the surface at CHeB, in order to apply Eq. 3.4 (with t' =CHeB and t =ZAMS) to obtain the field strength at the surface of the stripped star at CHeB. Thus, we are assuming that the field's strength and geometry are not affected by the mass transfer event, during which the stars retain all magnetic energy and field lines. The results are presented in the top panel of Fig. 4.1, which shows the surface field value at CHeB for given x values as a function of the ZAMS field's strength. We find that the value of the initial field that yields a CHeB field strength above the observational upper limit of Eq. 1.2 (represented by the red shaded area in the plot)

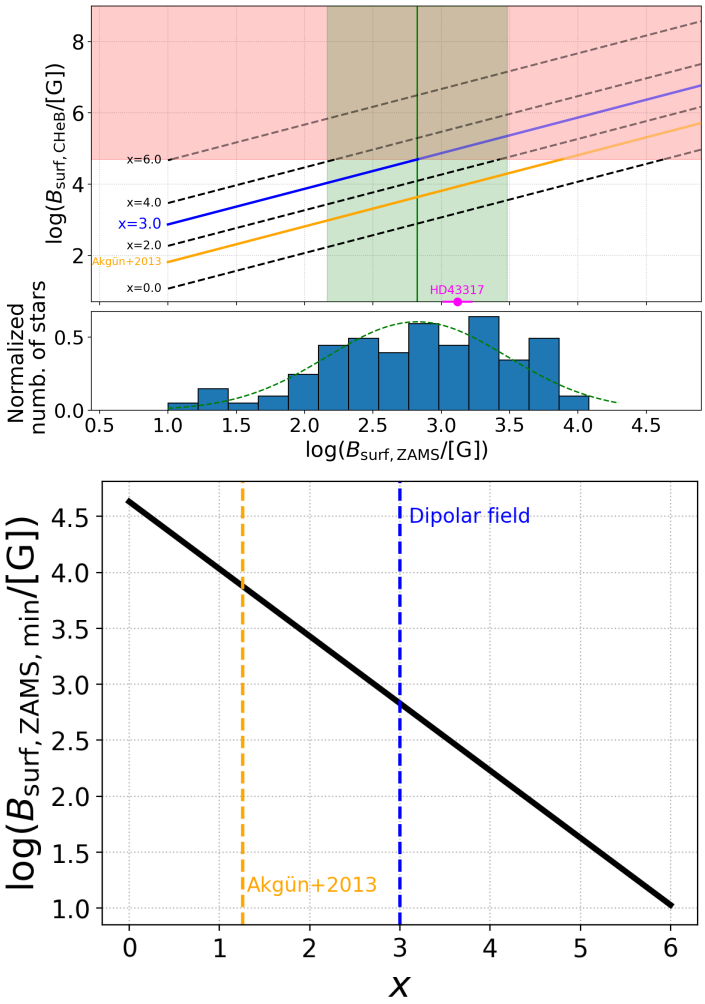

Figure 4.1: Initial parameters variation for the poloidal field topology. (Top panel) Surface field strength after stripping as a function of the initial surface strength parameter for different x parameters, with the addition of the field geometry from Akgün et al. (2013) (orange line). The CHeB field values above the observational upper limit are indicated by the red shaded area, while the magenta dot represents the surface field strength of HD43317, which is the only star for which a magneto-asteroseismic model exits (Lecoanet et al. 2022). The histogram represents the B-type observed fields from the Makarenko et al. (2021) sample, the Gaussian fit average of which is shown in the top plot by the vertical green line, with the $\pm 1\sigma$ region shaded. (Bottom panel) Minimum value of the field strength at ZAMS required to obtain a CHeB surface field above the conservative upper limit for each value of the x parameter. The vertical dashed lines show the x value of the most important geometries, that are the dipolar (blue) and the poloidal+toroidal of Akgün et al. (2013) (orange).

for the dipolar field is $\log(B_{\rm surf,ZAMS,min}/[\rm G]) = 2.82$, that exactly matches the average field strength $\langle \log(B_{\rm obs}/[\rm G]) \rangle = 2.82 \pm 0.65$ obtained by Makarenko et al. (2021) via a Gaussian fit of their observational sample (represented by the green line in the plot). This means that, assuming the dipolar geometry, the average field observed would lead to a field strength after the stripping similar to our observational upper limit. For other values of x, the minimum values of the initial field that yield a CHeB field above the

observational upper limit are shown in the bottom panel of Fig. 4.1. As expected, the steeper the radial dependence, the lower the initial field required.

Nevertheless, the purely poloidal field configuration is a rather rough approximation, since it is known that it will be highly unstable (Markey & Tayler 1973; Wright 1973) and will thus not survive long enough to be still present at CHeB. A possible way to produce a long-lived configuration is to introduce a toroidal component to the purely poloidal field. Already in the pioneering work of Prendergast (1956) it was shown analytically that adding to the poloidal field inside the star a surrounding toroidal field of similar strength yields an exact solution of the equations of hydromagnetic equilibrium. Thus, this poloidal+toroidal configuration represents a spherical equilibrium configuration. An intuitive explanation of why this happens was given by (Flowers & Ruderman 1977): the internal fluid motions reduce the external field energy of the poloidal component, but in doing so, they also twist the toroidal component, increasing the total field energy. Numerical simulations suggested that the poloidal+toroidal configuration can be stable inside stars (Braithwaite & Spruit 2004; Braithwaite & Nordlund 2006; Becerra et al. 2022a,b). To investigate how much the results obtained for a purely poloidal geometry would change if we assumed the stable geometry, we repeat the calculations adopting the analytical formulation of such a configuration, based on the numerical simulations by Braithwaite & Spruit (2004), proposed by Akgün et al. (2013). In spherical coordinates, this formulation is expressed as

$$\mathbf{B} = \mathbf{B}_{\rm pol} + \mathbf{B}_{\rm tor} = B_0(\eta_{\rm pol}\hat{\nabla}\hat{\alpha}\times\hat{\phi} + \eta_{\rm tor}\hat{\beta}\hat{\nabla}\phi)\,, \tag{4.2}$$

where $\eta_{\rm pol}$, $\eta_{\rm tor}$ are dimensionless constants that determine the relative strengths of the two components and defining, for $x = r/R_{surf,ZAMS}$ and $a_{\rm pol} = B_0\eta_{\rm pol}$, $a_{\rm tor} = B_0\eta_{\rm tor}$:

$$\hat{\alpha}(x,\theta) = f(x)\sin^2\theta\,, \tag{4.3}$$

$$\mathbf{B}_{\rm pol} = a_{\rm pol}\hat{\nabla}\hat{\alpha}\times\hat{\phi} = a_{\rm pol}\left[\frac{2f(x)\cos\theta}{x^2}\hat{\mathbf{r}} - \frac{f'(x)\sin\theta}{x}\hat{\boldsymbol{\theta}}\right]\,, \tag{4.4}$$

$$f(x) = \begin{cases} \frac{35}{8}x^2 - \frac{21}{4}x^4 + \frac{15}{8}x^6 & \text{for } x \le 1\,, \\ x^{-1} & \text{for } x > 1\,, \end{cases} \tag{4.5}$$

$$\mathbf{B}_{\rm tor} = a_{\rm pol}\hat{\beta}\hat{\nabla}\phi = a_{\rm pol}\hat{\beta}\frac{\hat{\boldsymbol{\phi}}}{r\sin\theta}\,, \tag{4.6}$$

$$\hat{\beta} = \begin{cases} (\hat{\alpha}-1)^2 & \text{for } \hat{\alpha} \ge 1\,, \\ 0 & \text{for } \hat{\alpha} < 1\,. \end{cases} \tag{4.7}$$

The poloidal field lines of this geometry are shown in Fig. 4.2, with the shaded gray area representing the location of the toroidal component.

In order to keep the magnetic field stable, the total energies of the poloidal and toroidal components need to be comparable (Markey & Tayler 1973; Wright 1973; Braithwaite & Spruit 2004; Becerra et al. 2022b). Therefore, the first step is to determine the values of $a_{\rm pol}$ and $a_{\rm tor}$ that ensure this condition. To calculate them, we equate the energies stored in the poloidal and toroidal components to find

$$\frac{1}{8\pi}\int|\mathbf{B}_{\rm pol}|^2 dV = \frac{1}{8\pi}\int|\mathbf{B}_{\rm tor}|^2 dV \;\Rightarrow\; a_{\rm tor} \simeq 7\times10^2\, a_{\rm pol}\,. \tag{4.8}$$

A consequence of this is that the maximum strengths of the two components are also comparable. The above relation allows us to keep only $a_{\rm pol}$ as the free parameter that determines the field strength. The magnitude of the field is strongly angle-dependent even on a shell of fixed radius r_0 (i.e. the surface $r_0 = R_{\rm surf}$). To avoid this arbitrariness,

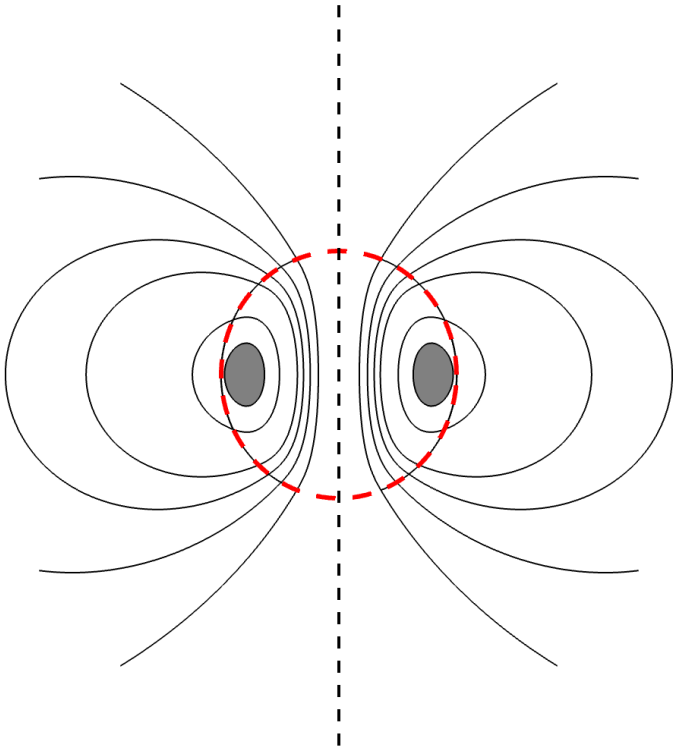

Figure 4.2: Field lines, i.e. lines of constant $\hat{\alpha}$, of the poloidal component of the stable geometry proposed by Akgün et al. (2013). The shaded gray area represents the donut-shaped region where the toroidal component is present. The dashed red line represents the stellar surface.

we calculate the field strength by integrating the field magnitude over a spherical surface as

$$\langle|\mathbf{B}|\rangle = \frac{1}{4\pi r_0^2}\int |\mathbf{B}| d\Omega_{r_0} = \frac{1}{4\pi}\int_0^{2\pi} d\phi \int_0^{\pi} |B(r,\theta)| \sin\theta d\theta \,, \tag{4.9}$$

where Ω_{r_0} is the solid angle at fixed radius r_0. We substitute the field components of Eq. 4.4 and 4.6 into the integral and we calculate it at $r_0 = R_{\rm surf,ZAMS}$. This allows us to obtain the average initial field strength on the surface. To ensure consistency with the initial conditions used in the poloidal analysis discussed in the previous paragraph, we carefully choose a range of values of $a_{\rm pol}$ such that $\langle|\mathbf{B}_{\rm surf,ZAMS}|\rangle = B_{\rm surf,ZAMS}$. We then follow the same steps as above to obtain the average field strength on the surface of the stripped star, with the results summarized by the orange line in Fig. 4.1. For this peculiar field geometry, we notice that the minimum initial field at ZAMS needed to obtain a CHeB field value above the observational upper limit is $\langle|\mathbf{B}_{\rm surf,ZAMS,min}|\rangle = 8\,$kG, that is one order of magnitude bigger than what we obtain for the dipolar geometry and towards the higher limit of the observational sample of B-type star.

4.2 Convective core hypothesis (II)

The magnetic field in massive stars may also be generated by a dynamo operating in the convective layers. From stellar evolution theory, we know that all stars more massive than $\sim 1.1\,M_\odot$ present a convective core during the main-sequence, inside which a magnetic dynamo is hosted. The dynamo mechanism converts a fraction of the kinetic energy of convection into magnetic energy, sustaining the resulting magnetic field against dissipation (Brandenburg & Subramanian 2005). The efficiency of this process, and thus

the amplitude of the generated magnetic field, depends on the importance of rotation in the star. This is because the dynamic balance between rotation and convection influences the ability of convection to generate a sustained field. This dependence can be quantified with the Rossby number Ro, which is defined as the ratio between inertial and Coriolis forces. For $Ro \lesssim 1$ (Augustson et al. 2016) an efficient dynamo is expected. The generated field has an equipartition strength, meaning that the magnetic energy $E_{mag} = B^2/8\pi$ and the kinetic energy of convection $E_K = \rho v_{\rm conv}^2/2$ are comparable, yielding

$$B_{\rm eq} = \sqrt{4\pi\rho v_{\rm conv}^2}\,, \tag{4.10}$$

where ρ is the density and $v_{\rm conv}$ the convective velocity. This result arises from the force balance between inertial and Lorentz forces in a weakly rotating system (Augustson et al. 2016). Since we apply this hypothesis to our non-rotating models, in our case $Ro \ll 1$: however, equipartition is still a good approximation, since Augustson et al. (2016) showed that even for very small values of Ro, the deviation from equipartition is less than one order of magnitude.

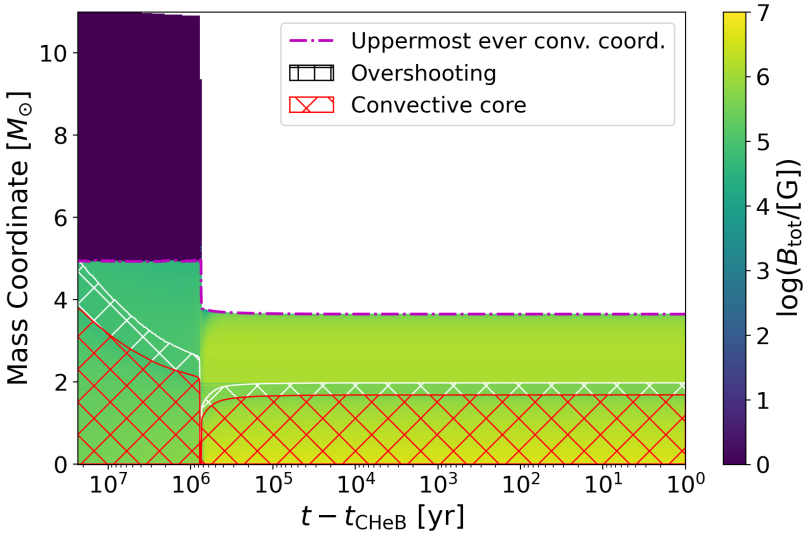

Figure 4.3: Kippenhahn diagram showing the evolution of the magnetic field strength left behind by the convective dynamo inside the star as a function of time before CHeB stage. The colorbar shows the field strength generated either by convection (inside the core) or frozen (in the radiative layers). The red hatched region indicates the convective core, while the white one the overshooting layer. The dash-dotted magenta line shows the uppermost mass coordinate that was ever convective.

Applying the convective dynamo to our non-rotating model yields the results shown in the Kippenhahn diagram of Fig. 4.3. Inside the convective core, indicated by the red hatched area, the equipartition field reaches up to 10^5 G in the main-sequence and 10^6 G in the He-burning core after the stripping. Since the white line represents the limit of the convective region (including the overshooting), it is clear that there is no convection on the surface of the stripped star, due to a small portion of the radiative envelope being retained. Thus, accounting only for the field generated by ongoing convection, we would not observe a surface field. The colorbar of the Kippenhahn diagram, however, evidently shows a field in the retained portion of the radiative envelope. This happens because we adopted the common assumption of the "frozen" field in radiative layers (Cantiello et al. 2016; Skoutnev & Beloborodov 2025): when the core retreats during the main-sequence, any mass shell that ever hosted a dynamo will retain the field it had the last time it was convective. Such field is "frozen" in the layer that is now radiative and keeps its strength

throughout the following evolution of the star. In practice, for every mass coordinate, this corresponds to ideally drawing a horizontal line in the Kippenhahn diagram and checking if it intersects the convective region for any time coordinate. In addition, since the field is now stably present in the radiative envelope, it will be subject to the flux freezing condition, thus Eq. 3.4 must be applied to every non-convective mass coordinate at CHeB to obtain the surface field strength. It is important to make two remarks: first, we do not apply the amplification factor to the He-burning core, since the new dynamo ignited by ongoing convection generates a stronger field that erases any frozen one left by main sequence convection; second, we can confidently assume that there will be a field on the surface at CHeB since the highest mass shell reached by the convective core during the mains sequence is above the surface shell of the stripped star. This is clearly shown by the dashed-dotted magenta line in Fig. 4.3, which indicates the uppermost shell that was ever convective.

Accounting for all these factors, the field expected at the surface of the stripped star at CHeB is $B_{\rm surf,CHeB} \simeq 10^5$ G – above the observational upper limit $B_{\rm max,CHeB} = 50$ kG. This value takes into account the considerations regarding the validity of the "frozen" field approximation against Ohmic diffusion made in Sect. 3.2. Even though direct calculation of the Ohmic timescale yields a short-lived field close to the surface, either through mass loss or magnetic buoyancy, a long-lived field can be brought to the surface in a very short timescale. This ensures the detectability of the field during the CHeB stage.

4.3 Rotational shear hypothesis (III)

Magnetic fields may also be generated in the radiative layers of stars by dynamos that operate without convection. In this section, we investigate the dynamo generated by differential rotation inside the radiative layer of a star, following the seminal work of Spruit (2002). Such a dynamo generates a field mainly in the layer between the rapidly, rigidly-rotating compact core and the slower-rotating envelope and it attains its energy from the star's rotation, meaning that the amount of available energy is limited. In this work, the main focus is the generated magnetic field that reaches the surface and can be detected after stripping. However, it is worth mentioning the broader significance of this field. In the literature, the primary interest lies in the internal torques that the field exerts on the core. These torques can reduce the degree of differential rotation and, in some cases, lead to uniform rotation. A schematic representation of Spruit dynamo is shown in Fig. 4.4. The dynamo cycle, as described by Spruit (2002), starts with a weak magnetic field in the radial direction δB_r (step a in figure), that is winded up by the shear layer generated by differential rotation (b) into an azimuthal field B_ϕ (c). The strength of the azimuthal component is much bigger than the initial radial field and increases linearly with time, up until it becomes unstable. At this point, Tayler instability (Tayler 1973; Spruit 1999) sets in, disrupting the azimuthal component to generate a new, weaker field in the radial direction (d) that then gets winded up again, restarting the cycle. After a few loops, the dynamo saturates when the winding up and decaying happen at the same rate (Braithwaite 2006), resulting in a field with components

$$B_\phi = rq\sqrt{4\pi\rho}\frac{\Omega}{N_{\rm eff}}\,, \qquad B_r = B_\phi q\left(\frac{\Omega}{N_{\rm eff}}\right)^2\,, \tag{4.11}$$

where ρ is the density, q the dimensionless differential rotation rate and Ω the star's rotation rate all calculated at radial coordinate r (Spruit 2002), with the azimuthal component being the dominant one. To account for the different compositions of the stratification in the stellar layer, the "effective" Brunt-Väisälä frequency $N_{\rm eff}$ was introduced, defined as

$$N^2_{\rm eff} \simeq \frac{\eta}{\chi}N^2_T + N^2_\mu\,, \tag{4.12}$$

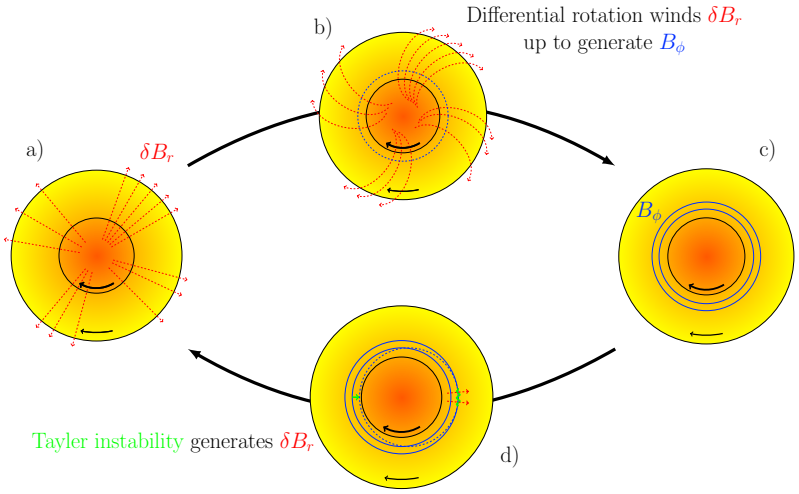

Figure 4.4: Schematic representation of the Spruit dynamo, as described by Spruit (2002).

where η is the magnetic diffusivity, χ is the thermal diffusivity, while N_T^2 and N_μ^2 are respectively the thermal and compositional components of the stratification.

Applying these equations to our rotating model with an initial surface rotation speed of $v_{\rm init} = 150\,{\rm km\,s^{-1}}$ yields the results shown in the top panel of Fig. 4.5. During the main sequence, the azimuthal field is generated not only in the shear layer between core and envelope, but also in the layers that were occupied by convection before the core's retreat. This is due to the compositional gradient left behind by convection. After the stripping, on the other hand, there are three main layers of field generation: two very thin shells, one at the core-envelope boundary above the overshooting region, the other halfway through the envelope, and the remains of the H-burning shell closer to the surface. In the first, the field reaches its peak strength of 10^5 G, just above the last convective mass shell. This layer is very thin and difficult to see in the plot. The greenish layer around $3.5\,M_\odot$ identifies the region occupied by the H-burning shell, where the azimuthal field reaches a strength of up to 10^4 G. In the deep blue layers, the Spruit dynamo cannot operate effectively. This is due to the condition for Tayler instability ($N_{\rm eff} > \Omega$) not being fulfilled in those layers. The exception is the tiny shell in the middle of the envelope, where a spike of compositional gradient leftover from the main-sequence. The condition $N_{\rm eff} > \Omega$ is also not fulfilled at the very surface of the star, mainly due to numerical artifacts connected to how MESA handles these quantities. Thus, to estimate the field strength on the surface, we first need to make some considerations: going deeper into the star, the condition is fulfilled and the field strength increases up to $|B| = \sqrt{B_r^2 + B_\phi^2} \simeq 2 \times 10^4$ G just above the H-burning shell. We calculate the mass loss magnetic buoyancy timescales and find that this field can rise respectively in a few years or in a few hours. Hence, in both cases, it can be detected on the surface. Its value is below the observational upper limit of Eq. 1.2 and thus we can not exclude the Spruit dynamo a priori.

This version of the Tayler-Spruit dynamo predicts larger rotation rates than what is expected from asteroseismology (Cantiello et al. 2014). A possible correction that predicts a higher saturation strength of the field, thus allowing spinning down the stars to lower rates, was proposed by Fuller et al. (2019): they argue that the weak radial field needs to be axisymmetric to be efficiently winded up by the shear layer, whereas the radial component generated by Tayler instability is non-axisymmetric. Thus, they introduce non-linear induction as a way to alter the weak radial component coming from Tayler instability and make it axisymmetric to close the dynamo loop. A schematic representation

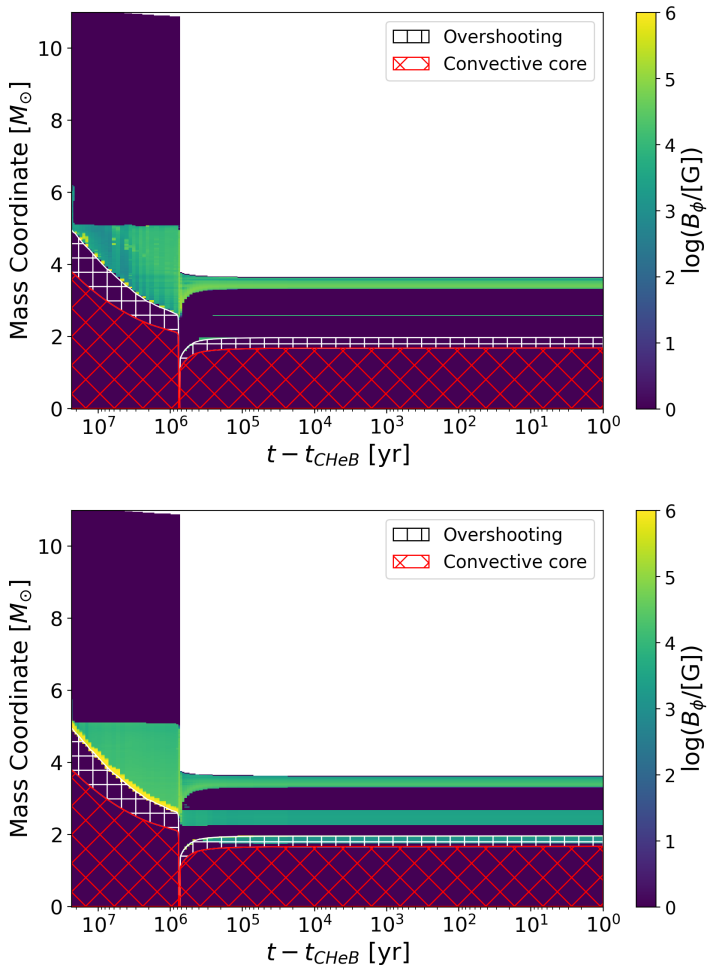

Figure 4.5: Kippenhahn diagrams showing the evolution of the structure of the star, represented by the mass coordinate. The colorbar shows the magnitude of the azimuthal field generated either by the Tayler-Spruit dynamo (top panel) or the Fuller dynamo (bottom panel). The red line hatched region shows the convective core, while the white one the overshooting layer.

of Fuller dynamo can be found in Fig. 4.6.

At saturation the field generated by the Fuller dynamo has components

$$B_\phi = \Omega\sqrt{4\pi\rho r^2}\left(\frac{q\Omega}{N_{\rm eff}}\right)^{1/3}, \quad B_r = \Omega\sqrt{4\pi\rho r^2}\left(\frac{q^2\Omega^5}{N_{\rm eff}^5}\right)^{1/3}, \tag{4.13}$$

where all the quantities are the same as in Eq. 4.11. Implementing the Fuller dynamo in MESA (following the prescription of Fuller et al. 2019) and applying it to our rotating model yields the results shown in the bottom panel of Fig. 4.5. As expected, the result resembles what was obtained from the Tayler-Spruit dynamo, just with a stronger field in the shear layer between core and envelope, represented by the bright yellow shell in the picture. Also in this case we can see three main field generation layers after the stripping, where the condition $N_{\rm eff} > \Omega$ is fulfilled. In this case, however, both the layer at the core-envelope boundary and the one in the middle of the envelope are more extended. The reason for this change traces back to the condition $N_{\rm eff} > \Omega$, as can clearly be seen in Fig. 4.7.

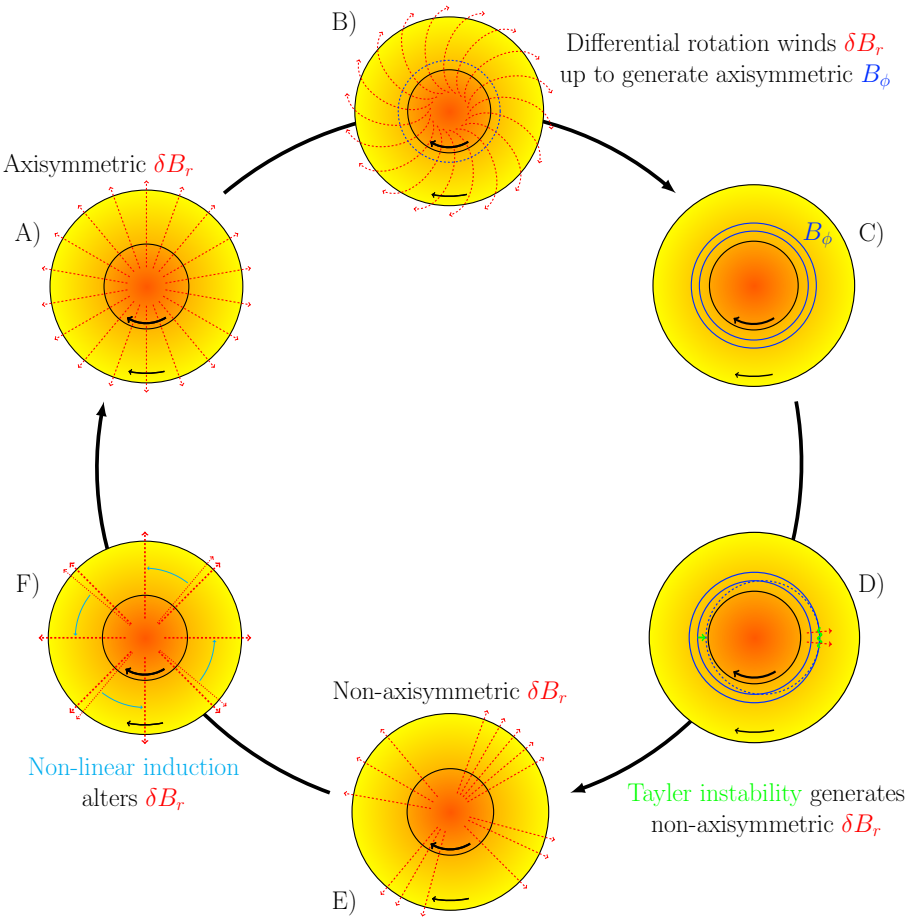

Figure 4.6: Schematic representation of Fuller dynamo, as described by Fuller et al. (2019). The "extra" step with respect to Spruit version is non-linear induction (E), that allows to restore the axisymmetry of the weak radial component δB_r.

Despite the $N^2_{\rm eff}$ profiles being the same in the Tayler-Spruit and Fuller cases, the latter damps the rotation rate more, as expected. Thus, Ω^2 is roughly two orders of magnitude lower, allowing for larger field generation regions. Applying the same considerations of the Tayler-Spruit case, we find that in the layer above the H-burning shell (that is found at around $3.5\,M_\odot$) the field strength decreases as we approach the surface, where the condition $N > \Omega$ is not fulfilled. Thus, for the Fuller dynamo the field that we expect to observe on the surface has magnitude $|B| = 9.2 \times 10^3$ G, which is below the observational upper limit of Eq. 1.2 and as a consequence cannot be excluded under our current approximations.

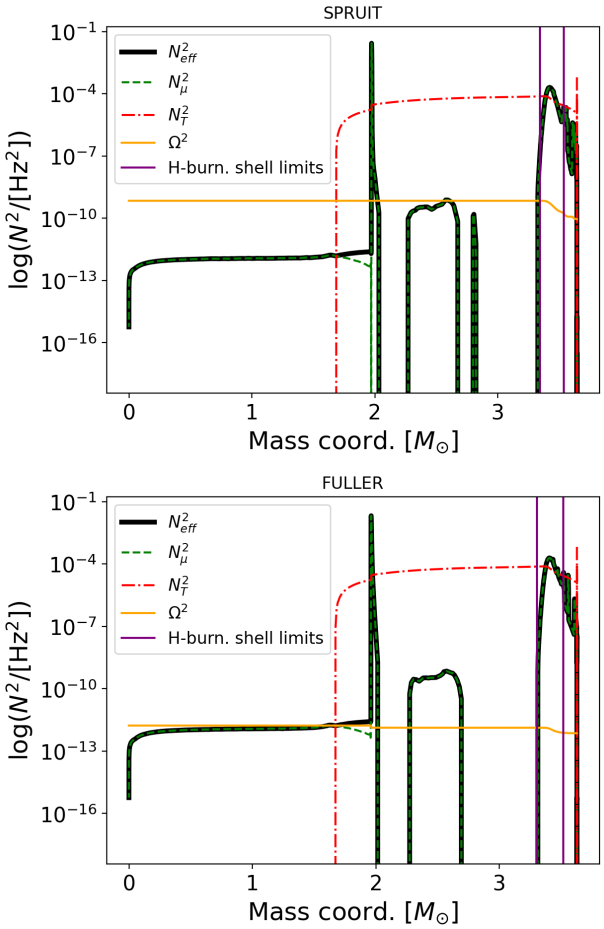

Figure 4.7: Profile plots of the effective Brunt-Väisäla frequency (black), its compositional (green) and thermal (red) components and the star's rotation rate (orange) as a function of mass coordinate at CHeB. In the top panel for the Tayler-Spruit dynamo, in the bottom panel for the Fuller dynamo.

Chapter 5

Results and Implications

	Fossil field hypothesis			Convective core hypothesis	Rotational shear hypothesis	
	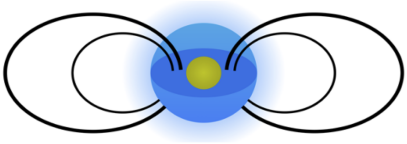			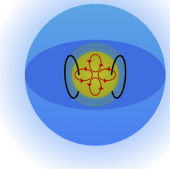	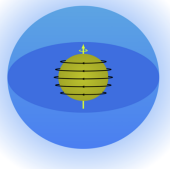	
	Uniform field ($x = 0$)	Dipolar field ($x = 3$)	Poloidal+torodial field configuration	Equipartition strength	Spruit dynamo	Fuller dynamo
References	//	//	*Braithwaite & Spruit 2004; Akgün 2013*	*Cantiello et al. 2016; Augustson et al. 2016*	*Spruit 1999; Spruit 2002*	*Fuller at al. 2019*
$B_{\mathrm{surf,ZAMS,min}}$ [G]	$4{\times}10^4$	$6.7{\times}10^2$	$8{\times}10^3$	N/A	N/A	N/A
$B_{\mathrm{surf,CHeB}}$ [G]	*(limit)*	*(limit)*	*(limit)*	$1{\times}10^5$ (excluded)	$\simeq 2{\times}10^4$	$\simeq 9{\times}10^3$

Table 5.1: Summary of obtained results

In Table 5.1 we summarize our findings. For the fossil field hypothesis, in which we assume the presence of a large-scale magnetic field already during the main sequence, we find that the magnitude of the surface field after stripping strongly depends on the choice of initial field strength and geometry. For a purely dipolar field (i.e. with radial dependence $B(r) \propto r^{-3}$) the initial strength that yields an after-stripping field above the observational upper limit is $B_{\mathrm{surf,ZAMS,min}} = 6.67 \times 10^2$ G, that exactly corresponds to the observed average field strength of the magnetized B-type stars sample of Makarenko et al. (2021). On the other hand, assuming the poloidal+toroidal field geometry of Akgün et al. (2013), the minimum shell-averaged field at ZAMS required to obtain a CHeB value above the limit is $B_{\mathrm{surf,ZAMS,min}} = 7.7 \times 10^3$ G, that falls towards the higher limit of the parameter space, comprising $\sim 95\%$ of the stars in the observational sample. However, considering a reasonable initial field strength of 1 kG, the CHeB surface field yielded is $B_{\mathrm{surf,CHeB}} \lesssim 10^4$ G, that is very close to our observational upper limit. This suggests that a tighter constraint on the upper limit is necessary to further elaborate on the validity of this geometry. At the moment, it can be interpreted as a more conservative and realistic choice with respect to the dipolar field, given also its proven numerical stability.

It is of particular interest to compare our results with magneto-asteroseismic measurements of magnetic fields near the stellar core. First, we investigate the comparison with the magneto-asteroseismic model of HD43317 from Lecoanet et al. (2022). This star is significant in this context because it is a main-sequence B-type star, i.e. the direct ances-

tor of our stripped star. In their work, Lecoanet et al. (2022) started from the measured surface field value of 1.3 kG. Then, assuming a purely dipolar geometry, they infer a lower limit to the near-core field strength of 500 kG using asteroseismology. This value is roughly double the magnitude expected by only considering the radial dependence of the field's strength ($\simeq$ 200 kG). This estimate is consistent, accounting for the mass difference between the models, with our dipolar field estimate outside the core during the main-sequence ($\sim$ 100 kG).

For the fossil field hypothesis, we are assuming that the field's strength and geometry are not affected by the mass transfer event, during which the star retains all magnetic energy and field lines. This is similar to what assumed by Justham et al. (2006), albeit in a different framework. This approximation stems from the uncertainty regarding the fate of the field's strength during Roche-lobe overflow, a topic that has yet to be comprehensively addressed in the literature and lies beyond the scope of this work.

For the convective core hypothesis (II), assuming equipartition, we find a predicted field strength at the surface of the stripped star of 1.09×10^5 G that is stable against Ohmic diffusion. While the mass difference limits the fairness of a direct comparison, a qualitative assessment against the near-core field of RGs from (magneto-)asteroseismology remains informative. Such comparison, shown in Fig. 5.1, reveals good agreement between our estimate and both the strength range of (Bugnet et al. 2021; Fuller et al. 2015; Stello et al. 2016) and the samples of Deheuvels et al. (2023) and Li et al. (2023). Since

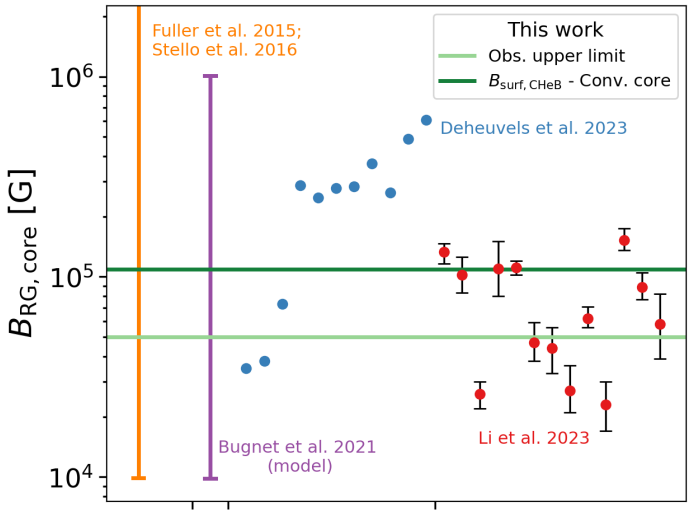

Figure 5.1: Near-core magnetic field strength of RGs inferred via asteroseismic models. The theoretical field ranges were found by Fuller et al. (2015); Stello et al. (2016) (orange) and Bugnet et al. (2021) (purple), while the points come from the samples of Deheuvels et al. (2023) (blue) and Li et al. (2023) (red, with errorbars). The horizontal lines in the shades of green represent the estimates of the surface field of a stripped He-star found in this work for the convective core and the observational upper limit.

our estimate is above the observational upper limit of Eq. 1.2, under our approximations this hypothesis can be excluded. However, further research is needed to investigate other field decay mechanisms that could weaken the surface field predicted.

Instead, for the rotational shear hypothesis (III) we find that the Tayler-Spruit dynamo and the Fuller dynamo yield respectively $B_{\mathrm{surf,CHeB,TS}} \simeq 2 \times 10^4$ G and $B_{\mathrm{surf,CHeB,F}} \simeq 9 \times 10^3$ G. Interestingly, the Fuller prescription is below the Tayler-Spruit one, despite being formulated as a way to increase the AM transport inside the star. This is, however,

not a surprise as the near-core field generated by the Fuller dynamo is in fact stronger than in the Tayler-Spruit case, but what we observe at the surface is the field above the hydrogen-burning shell, that is less affected by the higher AM diffusivity of the Fuller case. Nevertheless, both the fields are below the observational upper limit and are therefore not excluded under our approximations. A lower observational threshold would definitely improve the significance of this result, however is worth mentioning that the mainly toroidal nature of the field generated by these dynamos would prevent direct measurement via spectropolarimetry, which is currently the detection method that allows the best sensitivity, but only for longitudinal fields, i.e. the field component that is orthogonal to the surface.

Overall, under our current approximations, we can safely exclude only the convective core hypothesis (II), since the others yield field strengths below the observational limit. Thus, lowering the observational threshold is essential to further investigate the other hypotheses. Bringing the upper limit down by one order of magnitude would already significantly affect our conclusions. For example, it would help improve constraints on the geometry of fossil magnetic fields. Additionally, it could aid in distinguishing between the two dynamo mechanisms proposed in the rotational shear hypothesis. The outcome of such a distinction would also have important implications for our understanding of stellar rotation and angular momentum transport.

Conclusions

Motivated by the recent discovery of the first observational sample of binary-stripped helium stars, which also provided the first observational upper limit on their magnetic fields, we present theoretical estimates for the surface magnetic field strength of such stars. These estimates were obtained using the stellar evolution code MESA. We investigated three different origin hypotheses for the field: fossil field (I), convective core (II) and rotational shear dynamo (III). We then compared the obtained values with the observational upper limit for the field of Sect. 1 in order to establish whether any of the hypotheses yield a field above said limit. This new limit was obtained from preliminary analysis of the spectra of system 6 of Götberg et al. (2023) and Drout et al. (2023).

For this star:

- we exclude equipartition strength as predicted by the convective core hypothesis. This implies that either equipartition is not reached, or that the field decays more than we modeled.
- The observations do not rule out the rotational shear hypothesis. However, for both the Tayler-Spruit and the Fuller dynamos, the field strengths are very close to the upper limit. This suggests that deeper observations can either soon lead to a detection, or to useful constraints on such dynamo theories.
- Assuming typical magnetic field values observed in B-type main-sequence stars, we find that fossil field yields estimates below the upper limit. Thus, we cannot exclude them a priori. Exploring different geometries shows how the topology of Akgün et al. (2013) is the most realistic.

In this work, we rely on strong but reasonable approximations, such as flux conservation and "frozen" field in radiative layers. This choice stems from the complexity of magnetic fields in stars and the uncertainties that are yet to be completely solved on such topic. In addition, we used only one star, as it provided the most evident field limit, but the same analysis could be applied more broadly if additional limits become available. Nevertheless, we hope that our findings will motivate prioritizing observational time to help constrain the theories, and will serve as a solid starting point for more sophisticated modeling of the hypotheses. In light of the proximity of some of our findings with the observational limit, especially for the rotational shear hypothesis, a more precise observational constraint could greatly improve our results. This may be achieved with higher-resolution spectra and, possibly, spectropolarimetric data. In addition, combining measurements of stellar rotation rates with observations of magnetic field strengths enables tighter constraints on angular momentum transport mechanisms and their connection to stellar magnetism. We believe that such an effort would be justified as binary-stripped stars represent a unique opportunity to shed light on the origin and characteristics of magnetic fields in massive stars. These topics are still unclear and could prove useful in a variety of aspects of stellar evolution. Ultimately, this line of research may provide key insights into some of the most fundamental processes driving

massive star evolution.

Bibliography

Aerts, C. 2014, Proceedings of the International Astronomical Union, 9, 154–164

Aerts, C. 2021, Rev. Mod. Phys., 93

Aerts, C., Christensen-Dalsgaard, J., & Kurtz, D. W. 2010, Asteroseismology, Asteroseismology, Astronomy and Astrophysics Library (Springer)

Aizenman, M., Smeyers, P., & Weigert, A. 1977, A&A, 58, 41

Akgün, T., Reisenegger, A., Mastrano, A., & Marchant, P. 2013, Monthly Notices of the Royal Astronomical Society, 433, 2445

Alfvén, H. 1942, Nature, 150, 405

Augustson, K. C. 2019, Magnetism in Massive Stars

Augustson, K. C., Brun, A. S., & Toomre, J. 2016, The Astrophysical Journal, 829, 92

Baibhav, V., Berti, E., Cardoso, V., & Khanna, G. 2018, Phys. Rev. D, 97, 044048

Becerra, L., Reisenegger, A., Valdivia, J. A., & Gusakov, M. 2022a, Monthly Notices of the Royal Astronomical Society, 517, 560

Becerra, L., Reisenegger, A., Valdivia, J. A., & Gusakov, M. E. 2022b, Monthly Notices of the Royal Astronomical Society, 511, 732

Bouvier, J., Matt, S., Mohanty, S., et al. 2014, Angular momentum evolution of young low-mass stars and brown dwarfs: observations and theory, ed. H. Beuther, R. Klessen, C. Dullemond, & T. Henning (University of Arizona Press), 433–450

Bowman, D. M. 2020, Asteroseismology of High-Mass Stars: New Insights of Stellar Interiors With Space Telescopes

Bowman, D. M. 2023, Astrophysics and Space Science, 368

Braithwaite, J. 2006, A&A, 449, 451

Braithwaite, J. 2012, Monthly Notices of the Royal Astronomical Society, 422, 619

Braithwaite, J. & Nordlund, A. 2006, A&A, 450, 1077

Braithwaite, J. & Spruit, H. C. 2004, Nature, 431, 819

Braithwaite, J. & Spruit, H. C. 2017, Royal Society Open Science, 4

Brandenburg, A. & Subramanian, K. 2005, Physics Reports, 417, 1

Bugnet, L. 2022, A&A, 667, A68

Bugnet, L., Prat, V., Mathis, S., et al. 2021, A&A, 650, A53

Buysschaert, B., Aerts, C., Bowman, D. M., et al. 2018, A&A, 616, A148

Cantiello, M. & Braithwaite, J. 2011, A&A, 534

Cantiello, M., Fuller, J., & Bildsten, L. 2016, The Astrophysical Journal, 824, 14

Cantiello, M., Mankovich, C., Bildsten, L., Christensen-Dalsgaard, J., & Paxton, B. 2014, The Astrophysical Journal, 788, 93

Chandrasekhar, S. 1960, Radiative transfer (Dover Publications)

Charbonneau, P. & MacGregor, K. B. 2001, The Astrophysical Journal, 559, 1094

de Mink, S. E., Pols, O. R., & Yoon, S. 2008, AIP Conference Proceedings, 990, 230

Deheuvels, S., Li, G., Ballot, J., & Lignières, F. 2023, A&A, 670, L16

Deheuvels, S., Ouazzani, R. M., & Basu, S. 2017, A&A, 605, A75

Drout, M. R., Götberg, Y., Ludwig, B. A., et al. 2023, Science, 382, 1287

Drout, M. R., Soderberg, A. M., Gal-Yam, A., et al. 2011, The Astrophysical Journal, 741, 97

Duncan, R. C. & Thompson, C. 1992, ApJL, 392, L9

Dziembowski, W. A., Gough, D. O., Houdek, G., & Sienkiewicz, R. 2001, Monthly Notices of the Royal Astronomical Society, 328, 601

Eldridge, J. J., Fraser, M., Smartt, S. J., Maund, J. R., & Crockett, R. M. 2013, Monthly Notices of the Royal Astronomical Society, 436, 774

Ferrario, L. & Wickramasinghe, D. 2006, Monthly Notices of the Royal Astronomical Society, 367, 1323

Flowers, E. & Ruderman, M. A. 1977, ApJ, 215, 302

Fuller, J., Cantiello, M., Stello, D., Garcia, R. A., & Bildsten, L. 2015, Science, 350, 423

Fuller, J., Piro, A. L., & Jermyn, A. S. 2019, Monthly Notices of the Royal Astronomical Society, 485, 3661

García, R. A., Ceillier, T., Salabert, D., et al. 2014, A&A, 572, A34

Glebbeek, E., Gaburov, E., de Mink, S. E., Pols, O. R., & Portegies Zwart, S. F. 2009, A&A, 497, 255

Gomes, P. & Lopes, I. 2020, Monthly Notices of the Royal Astronomical Society, 496, 620

Gough, D. O. & Thompson, M. J. 1990, Monthly Notices of the Royal Astronomical Society, 242, 25

Groh, J. H., Oliveira, A. S., & Steiner, J. E. 2008, A&A, 485, 245

Grunhut, J. H., Wade, G. A., Leutenegger, M., et al. 2012, Monthly Notices of the Royal Astronomical Society, 428, 1686

Götberg, Y., de Mink, S. E., McQuinn, M., et al. 2020, A&A, 634, A134

Götberg, Y., Drout, M. R., Ji, A. P., et al. 2023, ApJ, 959, 125

Hansen, C. J., Kawaler, S. D., & Trimble, V. 2004, Stellar interiors : physical principles, structure, and evolution (Springer-Verlag, New York)

Hasan, S. S., Zahn, J.-P., & Christensen-Dalsgaard, J. 2005, A&A, 444, L29

Hubrig, S., Vigna-Gómez, A., Järvinen, S. P., Schöller, M., & Ilyin, I. 2025, Monthly Notices of the Royal Astronomical Society: Letters, 541, L80

Jermyn, A. S., Bauer, E. B., Schwab, J., et al. 2023, The Astrophysical Journal Supplement Series, 265, 15

Justham, S., Rappaport, S., & Podsiadlowski, P. 2006, Monthly Notices of the Royal Astronomical Society, 366, 1415

Keszthelyi, Z. 2023, Galaxies, 11

Kippenhahn, R. & Weigert, A. 1967, Zeitschrift für Astrophysik, 65, 251

Landstreet, J. 2009, EAS Publications Series, 39, 1

Landstreet, J. D. 2014, Proceedings of the International Astronomical Union, 9, 311–320

Lecoanet, D., Bowman, D. M., & Van Reeth, T. 2022, Monthly Notices of the Royal Astronomical Society: Letters, 512, L16

Li, G., Deheuvels, S., Ballot, J., & Lignières, F. 2022, Nature, 610, 43

Li, G., Deheuvels, S., Li, T., Ballot, J., & Lignières, F. 2023, A&A, 680, A26

Loi, S. T. 2021, Monthly Notices of the Royal Astronomical Society, 504, 3711

MacGregor, K. B. & Cassinelli, J. P. 2003, The Astrophysical Journal, 586, 480

Makarenko, E. I., Igoshev, A. P., & Kholtygin, A. F. 2021, Monthly Notices of the Royal Astronomical Society, 504, 5813

Markey, P. & Tayler, R. J. 1973, Monthly Notices of the Royal Astronomical Society, 163, 77

Mathis, S. & Bugnet, L. 2023, A&A, 676, L9

Mathis, S., Bugnet, L., Prat, V., et al. 2021, A&A, 647, A122

McClintock, J. E., Narayan, R., Davis, S. W., et al. 2011, Classical and Quantum Gravity, 28, 114009

Mestel, L. 1965, in IAU Symposium, Vol. 22, Stellar and Solar Magnetic Fields, ed. R. Lust, 420

Mestel, L. 1968, Monthly Notices of the Royal Astronomical Society, 138, 359

Moe, M. & Di Stefano, R. 2017, The Astrophysical Journal Supplement Series, 230, 15

Moss, D. 1989, Monthly Notices of the Royal Astronomical Society, 236, 629

Mosser, B., Elsworth, Y., Hekker, S., et al. 2012, A&A, 537, A30

Osaki, Y. 1975, PASJ, 27, 237

Parker, E. N. 1955, ApJ, 121, 491

Parker, E. N. 1979, Cosmical magnetic fields. Their origin and their activity, Oxford Classic Texts in the Physical Sciences (Oxford: Clarendon Press)

Paxton, B., Bildsten, L., Dotter, A., et al. 2011, The Astrophysical Journal Supplement Series, 192, 3

Paxton, B., Cantiello, M., Arras, P., et al. 2013, ApJS, 208, 4

Paxton, B., Marchant, P., Schwab, J., et al. 2015, ApJS, 220, 15

Paxton, B., Schwab, J., Bauer, E. B., et al. 2018, The Astrophysical Journal Supplement Series, 234, 34

Paxton, B., Smolec, R., Schwab, J., et al. 2019, The Astrophysical Journal Supplement Series, 243, 10

Petit, V. & Oksala, M. E. 2025, arXiv preprint arXiv:2504.00179

Prendergast, K. H. 1956, ApJ, 123, 498

Reiners, A. 2012, Living Reviews in Solar Physics, 9

Reynolds, C. S. & Fabian, A. C. 2008, The Astrophysical Journal, 675, 1048

Rui, N. Z. & Fuller, J. 2023, Monthly Notices of the Royal Astronomical Society, 523, 582

Sana, H., de Mink, S. E., de Koter, A., et al. 2012, Science, 337, 444

Saxena, A., Pentericci, L., Mirabelli, M., et al. 2020, A&A, 636, A47

Schneider, F. R. N., Ohlmann, S. T., Podsiadlowski, P., et al. 2019, Nature, 547, 211

Schöller, M., Hubrig, S., Fossati, L., et al. 2017, A&A, 599, A66

Scuflaire, R. 1974, A&A, 36, 107

Skoutnev, V. A. & Beloborodov, A. M. 2025, Magnetic Webs in Stellar Radiative Zones

Smith, N., Li, W., Filippenko, A. V., & Chornock, R. 2011, Monthly Notices of the Royal Astronomical Society, 412, 1522

Spitzer, L. 1962, Physics of Fully Ionized Gases (Interscience, New York)

Spitzer, Jr., L. 1958, in IAU Symposium, Vol. 6, Electromagnetic Phenomena in Cosmical Physics, ed. B. Lehnert, 169

Spruit, H. C. 1999, Differential rotation and magnetic fields in stellar interiors

Spruit, H. C. 2002, A&A, 381, 923

Stello, D., Cantiello, M., Jim, F., et al. 2016, Nature, 529, 364

Stokes, G. 1851, Transactions of the Cambridge Philosophical Society, 9, 399

Tauris, T. M., Kramer, M., Freire, P. C. C., et al. 2017, The Astrophysical Journal, 846, 170

Tayler, R. J. 1973, Monthly Notices of the Royal Astronomical Society, 161, 365

Thompson, T. A., Chang, P., & Quataert, E. 2004, The Astrophysical Journal, 611, 380

Tout, C. A., Wickramasinghe, D. T., & Ferrario, L. 2004, Monthly Notices of the Royal Astronomical Society, 355, L13

Turolla, R., Zane, S., & Watts, A. L. 2015, Reports on Progress in Physics, 78, 116901

Unno, W., Osaki, Y., Ando, H., Saio, H., & Shibahashi, H. 1989, Nonradial oscillations of stars (University of Tokyo Press)

van der Sluys, M. V., Röver, C., Stroeer, A., et al. 2008, The Astrophysical Journal, 688, L61

Vidotto, A. A., Opher, M., Jatenco-Pereira, V., & Gombosi, T. I. 2009, The Astrophysical Journal, 699, 441

Vitale, S., Lynch, R., Veitch, J., Raymond, V., & Sturani, R. 2014, Phys. Rev. Lett., 112, 251101

Wade, G. A., Grunhut, J., Alecian, E., et al. 2013, Proceedings of the International Astronomical Union, 9, 265–269

Wade, G. A., Neiner, C., Alecian, E., et al. 2016, Monthly Notices of the Royal Astronomical Society, 456, 2

Walder, R., Follini, D., & Meynet, G. 2012, Space Sci Rev, 166, 145

Wang, C., Langer, N., Schootemeijer, A., et al. 2022, Nature Astronomy, 6, 480

Wendell, C. E., van Horn, H. M., & Sargent, D. 1987, ApJ, 313, 284

Wright, G. A. E. 1973, Monthly Notices of the Royal Astronomical Society, 162, 339

Zeeman, P. 1896, Verslagen en Mededeelingen der Kon. Academie van Wetenschappen, Afd. Natuurkunde, 5, 181

Zhang, S. N., Cui, W., & Chen, W. 1997, The Astrophysical Journal, 482, L155

Appendix A

Supplementary figures

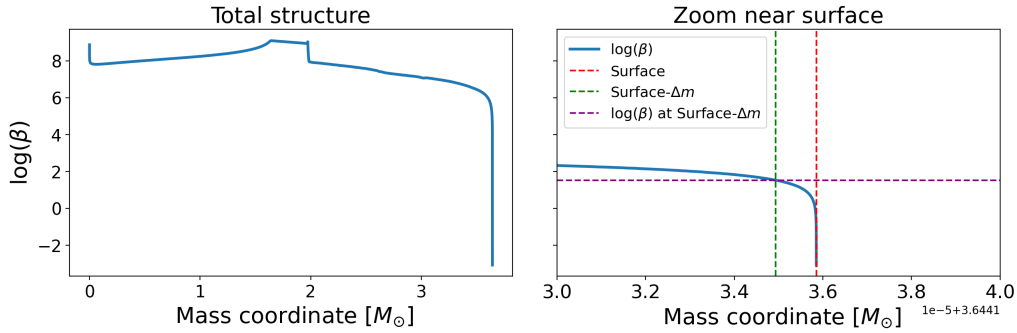

Figure A.1: (Left panel) Profile plot of the buoyancy β parameter, showing the behavior of the latter as a function of mass shell at CHeB stage. (Right panel) Zoom of the near surface behavior of the buoyancy β parameter at CheB stage. The vertical dashed lines show the surface shell (red), and the first shell at which $\tau_{\rm Ohm} > \tau_{\rm nuc,He}$ (green). The horizontal dashed purple line shows the intersection of the green line with the β profile.

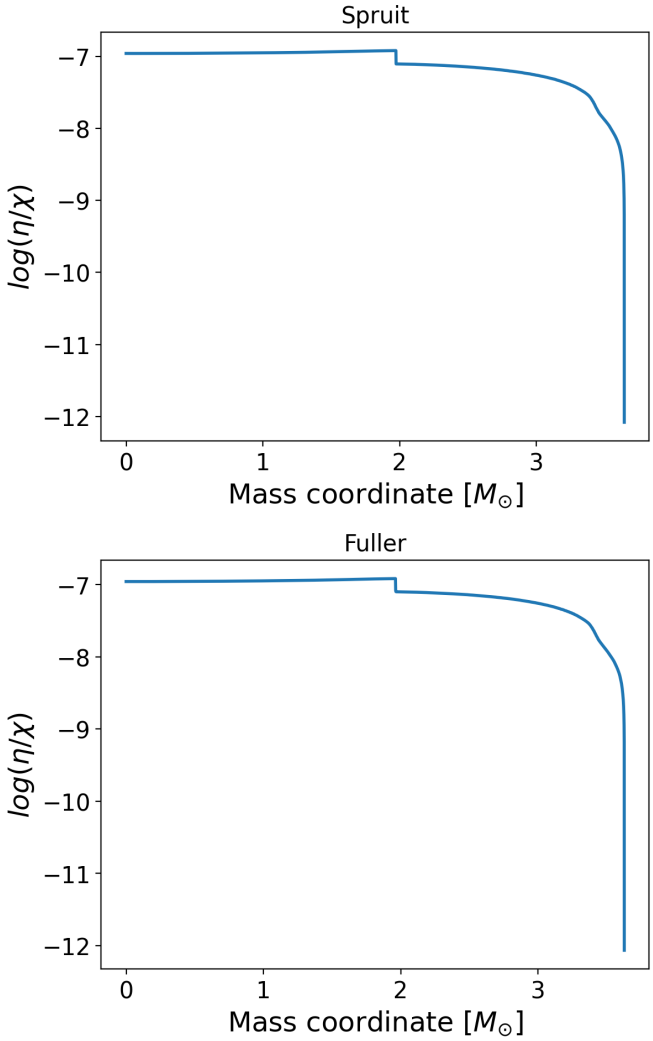

Figure A.2: Profile plots of the ratio between magnetic and thermal diffusivities as a function of mass coordinate at CHeB. In the top panel for the Tayler-Spruit dynamo, in the bottom panel for the Fuller dynamo.

Declaration

I hereby declare that this thesis is my own work, and that I have not used any sources and aids other than those stated in the thesis.

München, 14/07/2025

(Author's signature)